MAKING CROSSWALKS SMARTER: USING SENSORS AND LEARNING ALGORITHMS TO SAFEGUARD HETEROGENEOUS ROAD USERS

by

Yunchang Zhang

A Dissertation

Submitted to the Faculty of Purdue University

In Partial Fulfillment of the Requirements for the degree of

Doctor of Philosophy

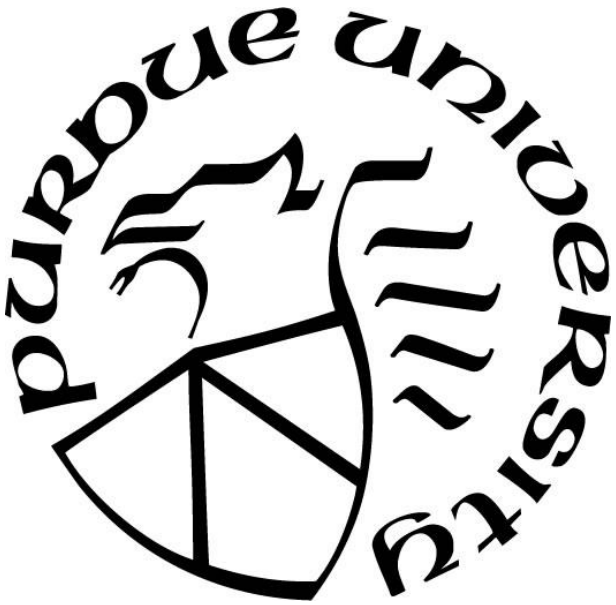

Lyles School of Civil Engineering

West Lafayette, Indiana

May 2022

THE PURDUE UNIVERSITY GRADUATE SCHOOL
STATEMENT OF COMMITTEE APPROVAL

Dr. Jon Fricker, Chair
Lyles School of Civil Engineering

Dr. Andrew Tarko
Lyles School of Civil Engineering

Dr. Yiheng Feng
Lyles School of Civil Engineering

Dr. Vincent Duffy
Department of Industrial Engineering

Approved by:
Dr. Dulcy Abraham

ACKNOWLEDGMENTS

This dissertation wouldn't be here if it weren't for some very important people in my life. Beginning with my mother (Mrs. Rongfen Sun), my father (Mr. Wenrui Zhang), and my cousins (Mr. Zhiwei Zhang, Mrs. Zhifeng Zhang, and Mrs. Jing Sun). There have been highs and lows, but you all have been standing behind me as always.

The journey to this dissertation began on a Wednesday morning with a meeting with my advisor, Dr. Jon Fricker, which I will never forget. My Ph.D. journey was made memorable by the videos Dr. Fricker showed me in our first meeting, his patience and humor, and his passion for teaching.

Moreover, both Dr. Andrew Tarko and Dr. Vincent Duffy served on my master's and doctoral dissertation committees. When we first met at Purdue, Dr. Yiheng Feng was invited to be a member of my doctoral dissertation committee. It is my sincere pleasure to thank you for your substantial support and guidance on my doctoral dissertation.

I have been encouraged, sustained, inspired, and tolerated by my beloved fiancée, Ruochen Yang. A Sunday afternoon hike began our tale, and the story continued with a starry night Perseid Meteor Shower watch. Now I'm looking forward to continuing our tale in Singapore for the next chapter.

TABLE OF CONTENTS

LIST OF TABLES

LIST OF FIGURES

ABSTRACT

The research described in this dissertation began in response to frequent questions from users of several crosswalks near a university campus. At each crosswalk was a sign indicating that motorists should yield to pedestrians in the crosswalk. That this message was not being interpreted uniformly was a concern at locations where heterogeneous road users (pedestrians, cyclists, and motorists) were interacting. Instead of trying to impose a single interpretation on users of each crosswalk, it was decided to observe and analyze interactions between users of the crosswalk.

Several hours of video were recorded of pedestrians and motorists "negotiating" the right of way at the crosswalk. Because these crossing locations were marked but not signalized, they were called "semi-controlled crosswalks". The negotiations took place during what were called pedestrian-motorist interactions (PMIs). The PMIs observed on video can be characterized as a "zebra-crossing" game, as described in Chapter 4 of this dissertation.

Recently, computer vision (CV) algorithms have been extensively used in road users' detection and tracking at an unparalleled spatial-temporal scale. In this study, CV algorithms have been applied to convert the video recordings into a large-scale spatial-temporal trajectory dataset including 800 pedestrians and cyclists interacting with more than 500 vehicles. Utilizing the trajectory dataset, a spatial-temporal graph convolutional network-based sequence to sequence (ST-GCN-Seq2Seq) algorithm has been developed to reasonably forecast heterogeneous road users' trajectories and behavior in real time. Combining CV and ST-GCN-Seq2Seq algorithms can help both design an intelligent tracking system and achieve a form of "smart" interaction at semi-controlled crosswalks for heterogeneous road users.

Based on road users' arrival patterns detected from CV algorithms, it is likely that a "smart" control strategy can minimize the delay of pedestrians and motorists at crosswalks. Therefore, another branch of this study is to investigate the "smart" control strategies at crosswalks using traffic signal controllers. A reinforcement learning framework was proposed as the "smart" control strategy, and several experiments were conducted using microsimulation. The proposed

reinforcement learning framework is able to reduce traffic delay (efficiency), considering real-time pedestrian flow rates and vehicle flow rates with appropriate sensors.

Keywords: Crosswalks; Pedestrian-Motorist Interaction; Heterogeneous Road Users; Learning Algorithms

1. INTRODUCTION

Semi-controlled crosswalks are shared spaces where ‘‘State Law Yield to Pedestrian Within Crosswalk’’ signs are presented. See Figure 1. Non-motorized road users (pedestrians and cyclists) at semi-controlled crossings have priority over approaching vehicles in Indiana. Nevertheless, observations indicate that confusion exists among pedestrians and motorists, because of varying interpretations of the R1-6 Sign:

1. Sometimes drivers stop and let pedestrians and cyclists waiting in the curb areas cross.
2. Sometimes drivers fail to yield to pedestrians entering the crosswalk.

Ambiguity arises. Instead of directly imposing a single interpretation, hours of videos were taken to observe heterogeneous road users’ behaviors and analyze heterogeneous road users’ interpretations of the R1-6 Sign.

Figure 1 R1-6 Sign at Semi-Controlled Crosswalk

Analyzing heterogeneous road users’ behaviors at semi-controlled crosswalks requires “numbers”. A road user detection and tracking system is developed to convert videos to a digital database with numbers. The road user detection and tracking system consists of two parts:

1. Detection module is used to detect heterogeneous road users and assign each detected road user a unique identification number.

2. Tracking module is applied to associate detections of a single road user across frames in a video sequence.

The road user detection and tracking modules generate a large-scale spatial-temporal trajectory dataset which is introduced in Section 3.1.

After converting video recordings into "numbers", heterogeneous road users' interpretations of the R1-6 sign message will be analyzed. A learning module consisting of three learning algorithms is proposed. The first learning algorithm is named "Zebra-Crossing Game".

1.1 Zebra-Crossing Game at Semi-Controlled Crosswalks

The zebra crossing game defines interactions between non-motorized road users (pedestrians and cyclists) and motorists. Due to varying interpretations of the R1-6 sign, pedestrians and motorists must rely on parties invoking "social rules" to establish priority for use at the site (Fricker and Zhang, 2019). For example,

1. Pedestrian-motorist interaction (PMI) Case 1: pedestrians will cross immediately if an approaching vehicle is far away from the crosswalk (Zhang et al., 2020); and
2. PMI Case 2: pedestrians will stop and let vehicles go first if a vehicle is too close to yield to the subject pedestrian in the crosswalk (Zhang et al., 2020).

Nevertheless, "social rules" can be ambiguous due to the lack of communication between road users. There are two cases of special interest:

3. PMI Case 3: if the interacted motorist is neither too far from the crosswalk nor too close (40 feet to 50 feet), the "negotiation" between a pedestrian and a motorist will be more complicated (the pedestrian does not cross, and the motorist yields) and result in some amount of delay (Zhang et al., 2020); and
4. PMI Case 4: if the subject pedestrian steps into the crosswalk, and the interacted driver does not yield to the pedestrian, it would be a dangerous situation (Zhang and Fricker, 2021a).

The PMIs (Case 1, Case 2, Case 3, and Case 4) at a semi-controlled crosswalk constitute a "zebra crossing" game involving two players – a pedestrian and a motorist. The definition of PMI is given in Chapter 3.2.

The four cases of PMI can be summarized as:

- PMI Case 1: the pedestrian crosses, and the driver yields.
- PMI Case 2: the driver does not yield, and the pedestrian waits in a curb area.
- PMI Case 3: the driver yields, and the pedestrian does not cross.
- PMI Case 4: the driver doesn't yield, and the pedestrian chooses to cross.

PMI Case 3 defines the confusion event that involves delay (efficiency issue), and PMI Case 4 defines conflict event that brings the safety issue. Therefore, confusion and conflict events are of special interest at semi-controlled crosswalks, and it is essential to model the "zebra-crossing game" to quantify the probabilities of confusion and conflict for operational and safety assessments.

To quantify players' actions, the PMI dataset is established using the trajectory dataset. The PMI dataset is introduced in Sections 3.1 and 3.2. The zebra-crossing game structure is described in Chapter 4.

1.2 Trajectory Prediction

The trajectory prediction is an extension of the first learning algorithm (zebra-crossing game). The zebra-crossing game considers players' final actions (pedestrian crossing decision and driver yielding decision) at a single time stamp. However, observations indicate that road users are involved in non-verbal (gesture, pose, etc.) communications over multiple time steps as they interact in shared spaces:

1. If there is a vehicle approaching the crosswalk, a pedestrian is likely to
    a. enter the curb area,
    b. wait for the response of the driver, and
    c. step into the crosswalk if the driver finally decelerates or stops.
2. If there is a pedestrian waiting in the curb area, a driver is likely to
    a. decelerate to give a signal to the pedestrian,
    b. wait for the response of the pedestrian, and
    c. accelerate to leave the crosswalk area if the pedestrian waves to the driver.

From the two cases shown above, pedestrian or cyclist crossing decisions and driver yielding decisions are sequential decision-making tasks involving interactions between heterogeneous road users over consecutive time steps. Time-related quantities (positions, speeds, and acceleration rates of road users) are likely to have significant impacts on road users' decisions (Rasouli and Tsotsos, 2019). The zebra-crossing game fails to capture consecutive interactions between heterogeneous road users, and an advanced computation model is required.

In addition, the zebra-crossing game only considers pedestrian-motorist interactions. Pedestrian-pedestrian interactions and hybrid interactions occur at semi-controlled crosswalks:

1. Pedestrian-pedestrian interaction (PPI) Case 1. pedestrians will respect personal spaces and keep safe distances from other pedestrians (Helbing and Molnar, 1995); and
2. PMI and PPI Case 2: pedestrians will include "safety in numbers" if one or more other pedestrians are present on the crosswalk or in the curb areas (Zhang and Fricker, 2021b).

To address multiple time interactions and hybrid interactions between heterogeneous road users, the second learning algorithm is introduced as a spatial-temporal graph convolutional network-based sequence to sequence (ST-GCN-Seq2Seq) model. ST-GCN-Seq2Seq predicts road users' future trajectories on the basis of observed trajectories and interactions between road users. Figure 2 reveals how ST-GCN-Seq2Seq works:

1. A frame from video recordings at time *t* is extracted. See Figure 2, and five heterogeneous road users (two pedestrians, one cyclist, and two drivers) are observed.
2. The trajectory dataset is accessed, and the most recent three-second trajectories of heterogeneous road users (blue-solid lines in Figure 2a) are extracted as observed trajectories.
3. ST-GCN-Seq2Seq utilizes the observed trajectories and encodes interactions between heterogeneous road users as input to predict future three-second trajectories of heterogeneous road users (red dotted lines in Figure 2b).

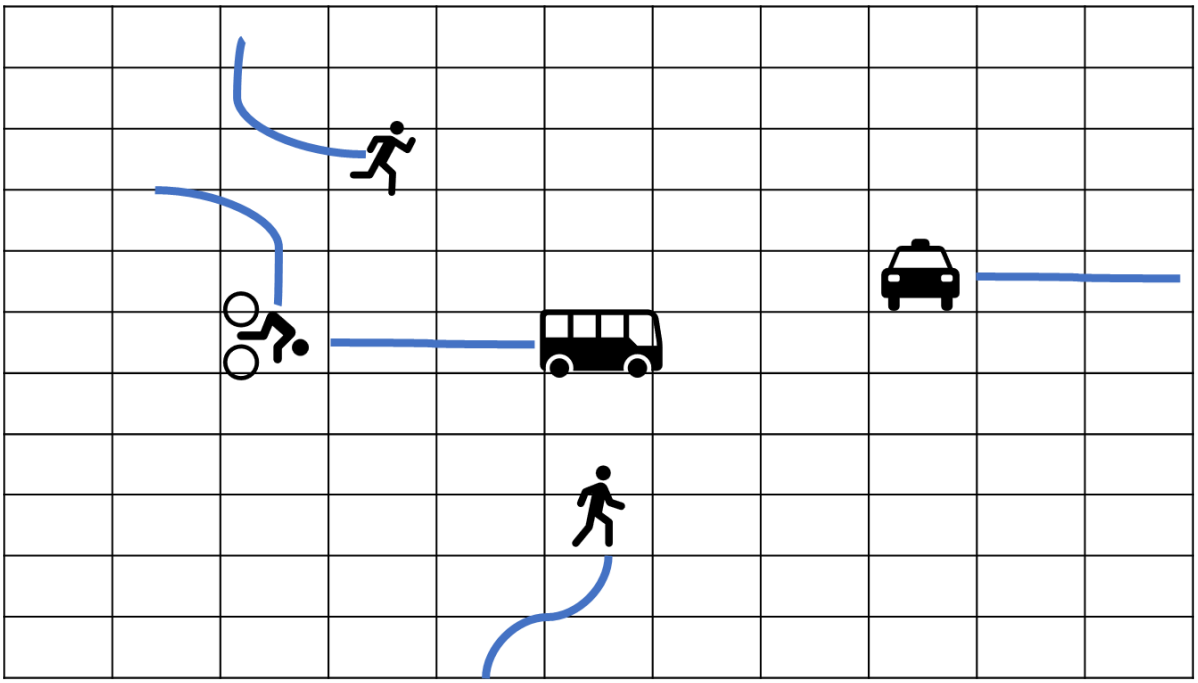

a. Observed Trajectories

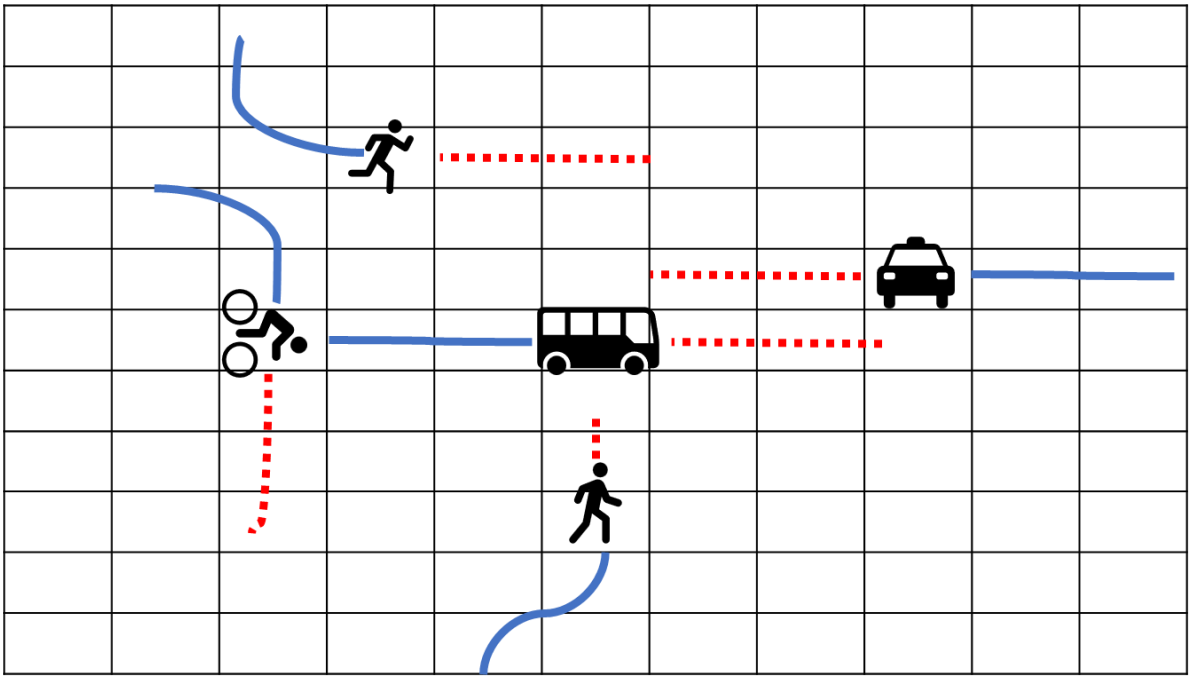

b. Predicted Trajectories

Figure 2 A Visualization of Motion Predictions

The trajectory profile is introduced in Section 3.1. The ST-GCN-Seq2Seq structure is elaborated in Chapter 5.

1.3 Traffic Controls at Crosswalks

Because real-time road users' arrival patterns can be captured by the road user detection and tracking system, it is likely that a "smart" control strategy can minimize delay to pedestrians and motorists at crosswalks. The third learning algorithm is to explore smart control strategies at crosswalks considering the variability of traffic.

To address the confusion and safety issues (PMI Case 3 and Case 4 in Section 1.1), conversion from an uncontrolled crosswalk to a signalized crosswalk was recommended by researchers (Asaithambi et al., 2016; Zhang et al., 2020). At signalized crosswalks, classical traffic signal controllers (TSCs) such as fixed-time signal control using Webster's (Webster, 1958) method and pushbutton controls are commonly applied. Traditional TSCs are easy to implement because they are pretimed or programmed to follow a specific control logic.

However, the fixed time signal control ignores fluctuation of the traffic demand, which may result in traffic congestion if the signal is improperly timed. This is especially true at crosswalks at or near universities, where pedestrian arrival rates fluctuate widely. Between class time, the pedestrian flow has significant but short-lived peaks. Fixed-time control cannot guarantee priority to pedestrians when the pedestrian flow is heavy, which causes longer pedestrian delay. Moreover, even though pushbutton controls give priority (after some delay) to pedestrians when large numbers of pedestrians are present, they have been observed to seize priority from drivers, leading to increased vehicle delay and safety issues (Millard-Ball, 2018). Therefore, utilizing predefined or pre-programmed TSCs is unlikely to account for variability in traffic at signalized crosswalks. Two main research questions need to be addressed:

1. To what extent should we consider control strategies for crosswalks from the perspectives of efficiency and safety?
2. What is the optimal control strategy for signalized crosswalks to account for variations in real traffic demand?

1.4 Dissertation Structure

Figure 3 reveals the flowchart of the dissertation. This dissertation is organized as follows:

- Chapter 2 reviews the most recent studies on the "zebra-crossing" game at semi-controlled crosswalks, human motion and intention modeling in shared spaces, and traffic signal control strategies.
- Chapter 3 introduces the road-user detection and tracking system for data collection and data pre-processing.
- Chapter 4 describes the first learning algorithm, that is, a game-theoretical approach to analyze efficiency and safety at semi-controlled crosswalks on the basis of the PMI dataset.
- Chapter 5 explores the second learning algorithm that helps both design an intelligent tracking system and achieve a form of smart interaction at semi-controlled crosswalks.
- Chapter 6 investigates smart traffic-control strategies at signalized crosswalks on the basis of a reinforcement learning framework.
- Chapter 7 discusses implications involving sensor deployment and presents conclusions.

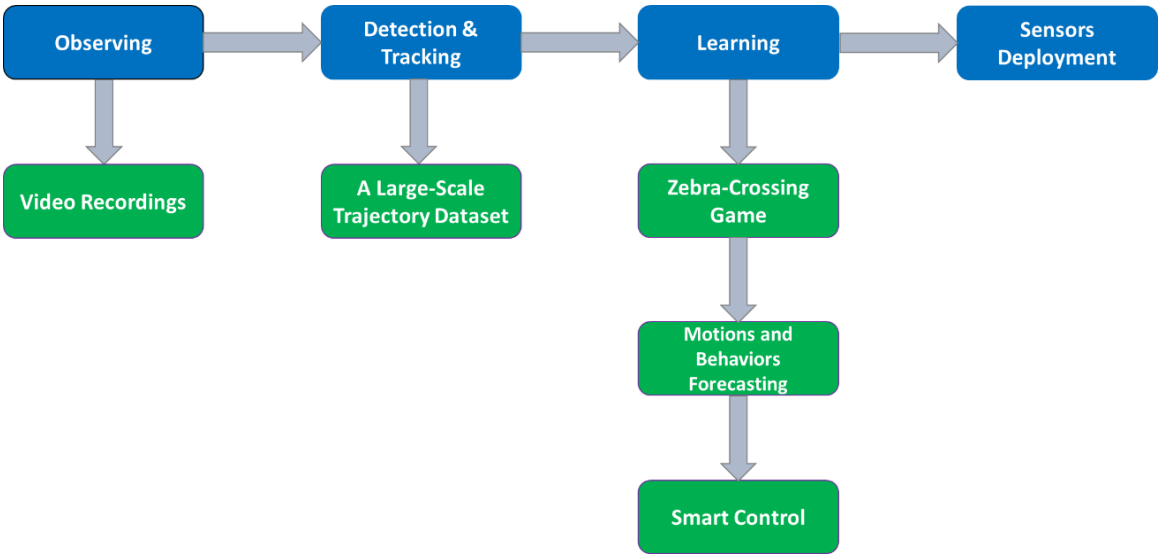

Figure 3 Dissertation Structure

2. LITERATURE REVIEW

2.1 Pedestrian-Motorist Interactions at Unsignalized Crosswalks

There is much literature on pedestrian-motorist interactions (PMIs) at unsignalized crosswalks. From observational experiments, a PMI can be extracted as an event based on the judgment of observer(s) (Fricker and Zhang, 2019).

2.1.1 Zebra Crossing Game

Discrete Choice Models

For pedestrian crossing behavior or driver compliance behavior, discrete choice models are often applied to estimate whether a pedestrian will accept (Y = 1) or reject (Y = 0) a gap if a PMI occurs. Generally, older and female pedestrians are more likely to wait in the curb area, hesitate before crossing, and maintain a lower speed while crossing at mid-block crosswalks (Cloutier et al., 2017; Sucha et al., 2017; Alver and Onelcin, 2018). Moreover, researchers (Pawar et al., 2015; Pawar and Patil, 2016; Fricker and Zhang 2019) have examined the impact of spatial or temporal gaps on pedestrian decision-making at semi-controlled crosswalks. Many of those studies conclude that vehicle dynamics, that is, the distance from a crosswalk to interacted vehicle and vehicle approach speed, are variables that significantly influence pedestrian crossing behavior. Furthermore, traffic and environmental factors, such as the number of lanes (Zhang et al., 2019), presence of countermeasures (Schroeder and Rouphail 2010; 2011), and crossing surface materials (Cloutier et al., 2017) have been proved to affect pedestrian crossing choices and driver's compliance behavior. A detailed review of the literature regarding PMIs can be found in Camara et al., (2020) and Amado et al., (2020), but the PMI at an unsignalized crosswalk is a "zebra crossing" game involving two players – pedestrian and motorist. The decision of one player is a response to the decision of the other. Consequently, considering only their individual decisions is not sufficient to describe the communication between the two players. The remedy is the game-theoretical approach that can assign a utility function to each combination of actions.

Game-Theoretical Approach

Only a few studies focus on the game-theoretical approach to modeling PMIs at unsignalized crosswalks. Elvik (2014) categorized ten classic games in road user behavior studies, but the game between a pedestrian and a motorist was not among them. Bjørnskau (2017) first developed a zebra crossing game with the perfect rationality assumption to explore the cyclist-vehicle interaction at unsignalized crosswalks in Norway. Two kinds of Nash Equilibria (Cycle/Yield and Yield/Driver) were found based on ordinal responses. Field observations confirmed that Cycle/Yield was the perfect Nash Equilibrium (NE) and was the most frequent solution in the real world. However, the Walk/Yield solution (the cyclist gets off the bike, negotiates with the driver, and walks over the crosswalk) is not a Nash Equilibrium solution. The Walk/Yield outcome implies that cyclists may not know whether the interacted driver is aggressive or not. A recent study of pedestrians and motorists at unsignalized crosswalks (Fricker and Zhang, 2019) frequently observed the Walk/Yield solution. Therefore, some real behaviors of pedestrians and motorists are missing in the NE with complete information. To capture uncertainties in the decision-making process, evolutionary game theory has been adopted, assuming players are not perfectly rational. Chen et al. (2016) integrated evolutionary game theory with cumulative prospect theory (CPT) in modeling PMIs at unsignalized crosswalks. The proposed evolutionary game framework has the potential to model the phenomenon of behavioral differences among pedestrians in a group. However, the evolutionary game framework is incorporated into a microsimulation platform that introduces a large number of parameters to be calibrated. Therefore, it is difficult to generalize the evolutionary game framework when we consider more sophisticated PMI models (Talebpour et al., 2015). To address these limitations, modified game-theoretical models such as Quantal Response Equilibrium (McKelvey and Palfrey, 1995) have been developed. In Quantal Response Equilibrium (QRE), players are assumed to make decisions with the lowest perceived costs that are subject to errors. A recent study (Arbis and Dixit, 2019) applied the QRE to model the lane-changing "game" between an on-ramp driver and a mainline driver. Results revealed that the QRE can accurately model the expected number and variance of driving strategies when the lane-changing game occurs.

2.1.2 Human Motion and Intention Modeling

Physics-Based Models

Physics-based models such as Cellular Automaton (Gipps and Marksjö, 1985; Blue and Adler, 2001; Lu et al., 2016), Kalman Filter (Elnagar, 2001), and Social Force (Helbing and Molnar, 1995; Zeng et al., 2014; Fujii et al., 2017) models have been widely used to model pedestrian-pedestrian interactions and pedestrian-driver interactions in shared space environments. Parameterized functions of road-users' trajectories are pre-defined. Map information (borders of sidewalks and buildings) and dynamic environment cues (repulsive or attractive forces by surrounding agents) can be incorporated into physics-based models to reasonably explain the collective strategies as road users interact in real street crossings (Rudenko et al., 2020). Pre-defined physics-based models introduce a large number of parameters and observed trajectory data should be applied to calibrate model parameters. Therefore, the physics-based models can be categorized as the *model-sense-calibrate* procedure.

Pattern-Based Techniques

In the era of big data, the application of pattern-based approaches to motion predictions has attracted more research attention. Unlike the *model-sense-calibrate* procedure, pattern-based models directly fit parameters from the data by applying linear or non-linear function approximators instead of specifying parameterized functions. The pattern-based approaches can be categorized as the *sense–learn–predict* procedure. Using sequential models, pattern-based techniques are capable of capturing local motion patterns using stochastic process-based techniques; for example, the mixture of Gaussian Processes (Ellis et al., 2009; Joseph et al., 2011; Zhi et al., 2020) and hidden Markov models (Nascimento et al., 2009). In addition, long-term spatiotemporal dependencies of human motions can be learned via the Recurrent Neural Networks (RNN) and long short-term memory (LSTM) networks. Recently, RNN and LSTM-based architectures have become a popular modeling approach for predicting human motions (Alahi et al., 2016; Gupta et al., 2018; Vemula et al., 2018; Zhang et al., 2019) and vehicle motions (Kim et al., 2017; Deo and Trivedi, 2018; Li et al., 2019). Human or vehicle-vehicle interactions were encoded in the RNN/LSTM-based architectures using various strategies (e.g., social pooling in Alahi et al., 2016; convolutional social pooling in Deo et al. 2019; and graph-based convolutional

module in Li et al., 2019). Compared with physics-based models, RNN/LSTM-based architectures can better predict the motions of homogenous road users based on observed trajectories and interactions. Another branch of pattern-based approaches applied non-sequential models to human motion predictions. A summary of non-sequential models can be found in the survey by Rudenko et al. (2020).

Planning-Based Methods

Human motion prediction can be considered a sequential decision-making problem. The sequential decision-making problem can be categorized as the planning-based method because the subject agent is assumed to be boundedly rational and will choose a sequence of actions to minimize the subsequent costs in the future. The planning-based approach will either specify an explicitly defined cost function (forward planning approach – see González et al., 2015) or infer the unknown cost function that guides an agent's behavior based on real observations (inverse planning approach - see Ho et al., 2016), which can be summarized as the *sense-reason-behavior* diagram. If transition dynamics (e.g., navigating a vehicle or simulating a robot) can be acquired, forward-planning methods will be utilized to fit unknown parameters of a general-purpose model with observed data. A review of forward planning approaches can be found in the survey (González et al., 2015). If transition dynamics cannot be easily modeled (e.g., agent-agent interactions), inverse planning approaches will be generally adopted to approximate the cost function or reward structure that infers proper actions for the target agent to take. Inverse planning approaches, such as behavioral cloning from observations (Torabi et al., 2018), linear programming-based inverse reinforcement learning (IRF) (Previtali et al., 2016), Maximum Entropy IRF (Ziebart et al., 2009; Alsaleh and Sayed, 2020), and generative adversarial imitation learning (GAIL) (Kuefler et al., 2017; Li et al., 2017; Bhattacharyya et al., 2018) have been extensively applied in pedestrian, cyclist, and vehicle motion predictions.

2.2 Control Strategies at Signalized Crosswalks

This section will highlight the literature review of traffic signal control strategies in terms of mobility and safety.

2.2.1 Mobility

Traditionally, traffic signal controllers (TSCs) are pretimed or programmed by a specific control logic using Webster's method (Webster, 1958). Although fixed-timed TSCs are straightforward to implement, real traffic conditions are not considered. For decades, researchers have proposed adaptive traffic-signal control (ATSC) technology as practical alternatives to conventional TSCs based on versatile optimization techniques. Evolutionary algorithms such as genetic algorithms (Mikami and Kakazu, 1994; Lee et al., 2005; Ricalde and Banzhaf, 2017) have been extensively applied in ATSC. Other heuristic algorithms such as particle swarm optimization (Garcia-Nieto et al., 2013) and max-pressure algorithms (Wongpiromsarn et al, 2012; Varaiya, 2013; Gregoire et al., 2014) and self-organizing traffic control algorithms (Heylighen and Gershenson, 2004; Cools et al., 2013) are developed to address complex traffic signal timing optimization problems. In addition, large-scale adaptive traffic control systems such as OPAC (Gartner, 1983), SCOOTS (Hunt et al., 1981), SCATS (Lowrie, 1990), RHODES (Mirchandani and Head, 2001), ACS-Lite (Luyanda et al., 2003), and CRONOS (Boillot et al., 2006) have been proposed in the system-level signal control in urban areas. However, most of the ATCS consider aggregated flow consisting of multiple transportation modes, and each mode is treated equally. Priority rules such as priorities for pedestrians and transit, are overlooked (He et al., 2014). The multi-modal priority signal control system is required to address priority for vulnerable road users. In addition to offline optimization techniques, recently applied online learning algorithms have been explored for "smart" TSCs. Optimal control and reinforcement learning (RL) based algorithms such as temporal difference learning and tabular Q-learning have been investigated (Mannion et al., 2016; Yau et al., 2017). Instead of directly updating a Q-value table, the value-function-based, and policy-gradient-based RL algorithms are approximated by deep neural networks (Mousavi et al., 2017). Deep Q Network (Gong et al., 2020), actor-critic (Aslani et al., 2018) and deep deterministic policy gradient (Genders and Razavi, 2019) algorithms have also attracted research attention.

2.2.2 Safety

In addition to mobility, the implementation of TSCs should take safety metrics into consideration. Crash data is the primary resource to quantitatively evaluate the safety of TSCs.

Crash Data

The Highway Safety Manual (HSM) provides a two-step procedure to quantitatively evaluate the safety of signalized intersections (AASHTO, 2010):

1. Use national safety performance functions (SPFs) to predict the severity of crashes as the baseline; and
2. Crash modification factors (CMFs) examine the safety impacts of design alternatives or changes from baseline.

Based on crash data, SPFs are fitted, and CMFs have been widely applied to evaluate the safety impact of installations of InSync (Ma et al., 2016; Khattak et al., 2018), SURTRAC (Khattak et al., 2018), and SCATS (Dutta et al., 2010) at signalized intersections. Another prevailing approach applied statistical methods to:

1. investigate the relationship between influencing factors and crash frequencies at signalized intersections using Poisson-based models (Sacchi et al., 2016; Fink et al., 2016); and
2. identify the relationship between contributing factors and severity of accidents at a signalized intersection using multinomial regression models (Fink et al., 2016; Khattak et al., 2019).

However, accidents are rare events. Analysts have to wait multiple years until an adequate number of observations have been acquired (Mannering et al., 2016). To address the lack of crash data, traffic conflicts and surrogate safety measures have been applied in safety evaluation at intersections (Tarko, 2021).

Surrogate Measures of Safety

Surrogate safety measures (time-to-collision, post-encroachment time, and deceleration rate et al.) derived from trajectory profiles have been widely applied as an alternative to crash data (Gettman and Head, 2003; Gettman et al., 2008) in the safety analysis. Preliminary results revealed that surrogate safety measures can reasonably reflect the severity of observed traffic conflicts at signalized intersections. These pioneer studies greatly contributed to the development of the

surrogate safety assessment model (SSAM). In addition, recently developed traffic simulation software such as Simulation of Urban Mobility (SUMO) (Lopez, et al., 2018) and VISSIM (PTV Group, 2021) significantly reduced the cost to collect trajectory profiles. Trajectory profiles extracted from traffic simulation software can be efficiently transformed as input for SSAM, which allows researchers to search for optimal TSCs via a large number of testing scenarios generated in the traffic simulation software. Stevanovic et al. (2013) proposed a multi-objective framework to search for the optimal TSCs that reduce the number of conflicts and minimize traffic delay using VISSIM and SSAM. The framework was further generalized to address the tradeoff between different performance measures (efficiency, safety and environmental impacts). (Stevanovic et al., 2015).

2.2.3 Pedestrian Pushbutton Controls at Signalized Midblock Crossings

As an alternative to fixed-time control, a pushbutton is frequently installed near signalized midblock crossings. Many variants of the pushbutton control strategies were developed (FHWA, 2014), such as pedestrian light-controlled (Pelican), rectangular rapid flashing beacons (RRFB), pedestrian hybrid beacon (PHB), and pedestrian user-friendly intelligent (Puffin). Table 1 summarizes traffic signal plans using pedestrian pushbutton control strategies at midblock crosswalks (Wu et al., 2022).

The safety and efficiency of pushbutton control strategies have been investigated in the existing literature. Wu et al. (2022) investigated the effectiveness of the Pelican control strategy and concluded that Pelican control would give priority to pedestrians after each button activation, which significantly interrupted traffic flow.

As a modified version of Pelican, RRFB and PHB controls allow a vehicle to cross once the subject pedestrian(s) have already crossed the crosswalk during the flashing amber and flashing red phases in Table 1. Godavarthy and Russell (2016) compared the effectiveness between two PHB midblock crossings and one Pelican crosswalk. Results revealed that vehicle delay at PHB crossings was significantly lower than at a Pelican crosswalk. Additionally, a PHB had the highest driver compliance rate among midblock crossing treatments, with approximately 97% driver compliance (Fayyaz et al., 2019). In comparison, field experiments indicated a 57% driver

compliance rate for RRFB (Fayyaz et al., 2019). However, a case study in Washington D.C. indicated low pedestrian compliance rates (50%-66%) in PHB crossings due to the lack of understanding of the operations of PHB (Arhin and Noel, 2010). Pedestrians preferred to directly jaywalk without waiting for a pedestrian green phase or "WALK" signal (Marisamynathan and Vedagiri, 2018).

To balance pedestrian delay and motorist delay at midblock crossings, the Puffin control strategy is widely applied in Europe (Hassan et al., 2013). Both curb-side detection and on-crosswalk detection are included in the Puffin control system. Curb-side detection is utilized to confirm the presence of pedestrian(s) waiting within curb areas. If pedestrians leave the curb areas, it continues the vehicle green phase without interrupting traffic. On-crosswalk detection is used to confirm the presence of pedestrian(s) on the crosswalk. If there is at least one pedestrian on the crosswalk, and the signal phase is about to turn red, the extended pedestrian green phase (see Table 1) will be guaranteed.

Table 1 Summary of Pedestrian Control Strategies for Signalized Midblock Crossings

Controls	**Detectors**	**Signal Phase Sequence**
Fixed-Time	Not Applicable	
Pelican	Pushbutton	
RRFB	Pushbutton	
PHB	Pushbutton	
Puffin	Pushbutton and Camera	

3. DATA COLLECTION

This chapter will highlight data collection at two semi-controlled crosswalks and one signalized crosswalk at Purdue University.

Intersection 1: Video recordings were made in Spring 2017, when Grant Street was a one-way northbound street. The street had two 12-feet wide lanes with a speed limit of 25 mph. The crossing is primarily used by students walking to/from class and by faculty and staff walking from/to nearby parking garages. See Figure 4(a).

Intersection 2: Video recordings were made in Spring 2017, when North University Street was a one-way northbound street. The street had two 10-ft wide lanes (plus a 4-foot bicycle lane) with a speed limit of 25mph. See Figure 4(b). Video recordings were made at four different time periods, during which traffic volumes and pedestrian flows were observed.

(a) (b)

Figure 4 Semi-Controlled Crosswalk.
(a) Northbound Grant Street at Purdue Memorial Union, 2017.
(b) Northbound University Street, 2017.

3.1 Trajectory Profile

Computer vision algorithms have been applied to multi-object (pedestrian, cyclist, and vehicle) detection and tracking. Yolo-V3 and deep-sort algorithms have been used to convert the video recordings into a digital database with “numbers”.

3.1.1 Object Detection and Tracking

An example of pedestrian detection and tracking has been shown in Figure 5(a) and Figure 5(b). The red solid line in Figure 5(b) represents the extracted trajectory for subject pedestrian No. 27. The original Yolo-V3 and deep-sort algorithms can be found in the GitHub repository (https://github.com/ZQPei/deep_sort_pytorch). A modified version of the algorithms used in the study site can be found in our GitHub repository (https://github.com/YZhang-Genghis).

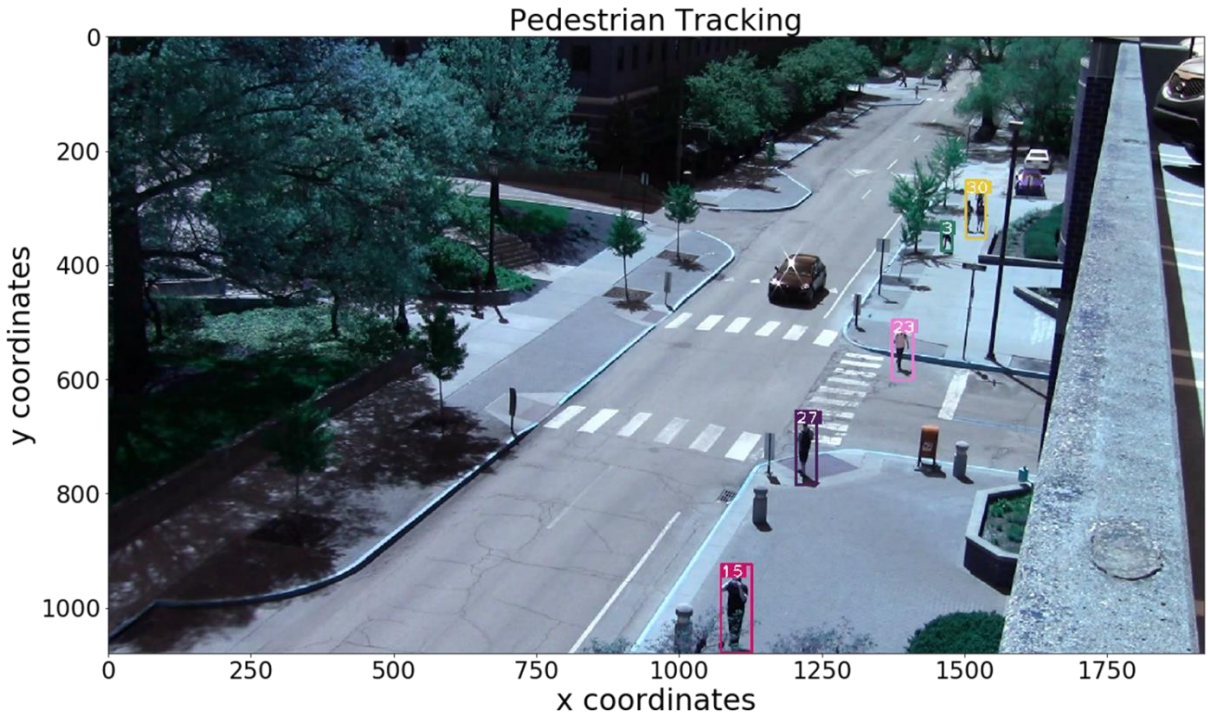

(a) An Example of the Pedestrian Detection Module

Figure 5 continued

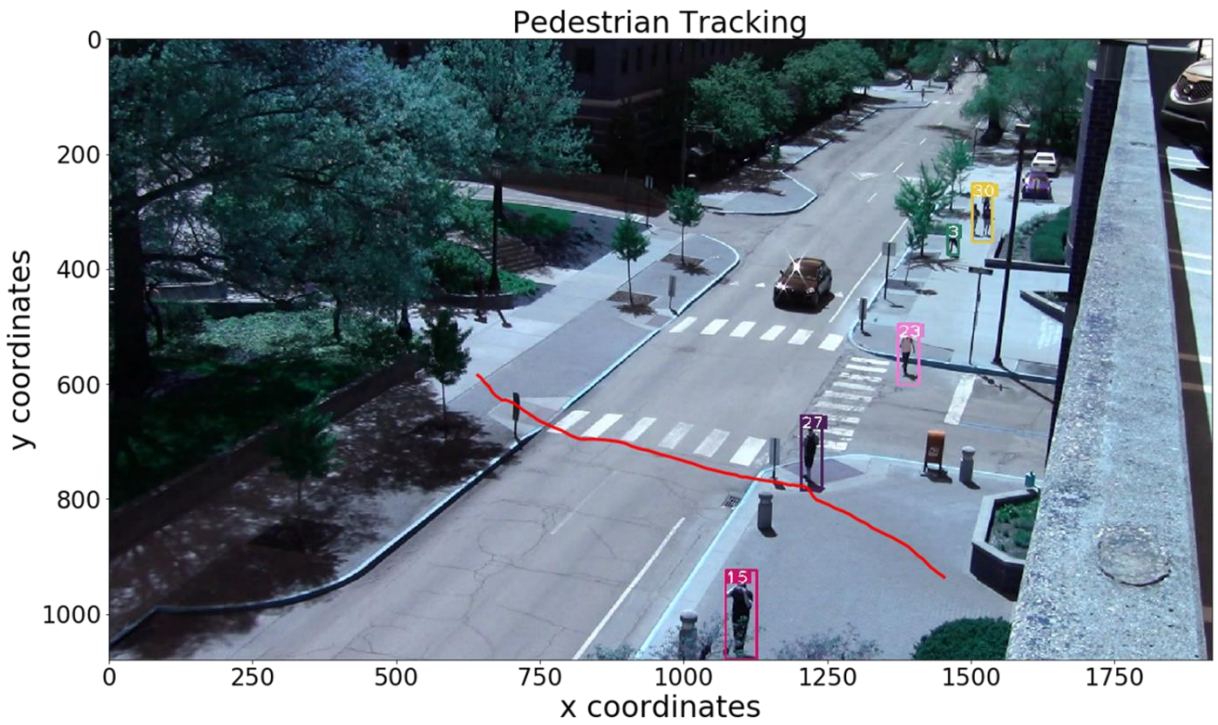

(b) An Example of the Pedestrian Tracking Module

Figure 5 Road User Detection and Tracking

3.1.2 Homography

After extracting pedestrian, cyclist, and vehicle trajectories, we project the dataset of trajectories from the camera view into the Google Map view to obtain the precise latitude and longitude maneuvers of agents. Consider two images of the intersection shown in Figure 6(a) and Figure 6(b), the four corresponding points in four different colors – red, green, orange, and blue dots represent the same physical points in the two images.

(a) Camera View of the Study Site

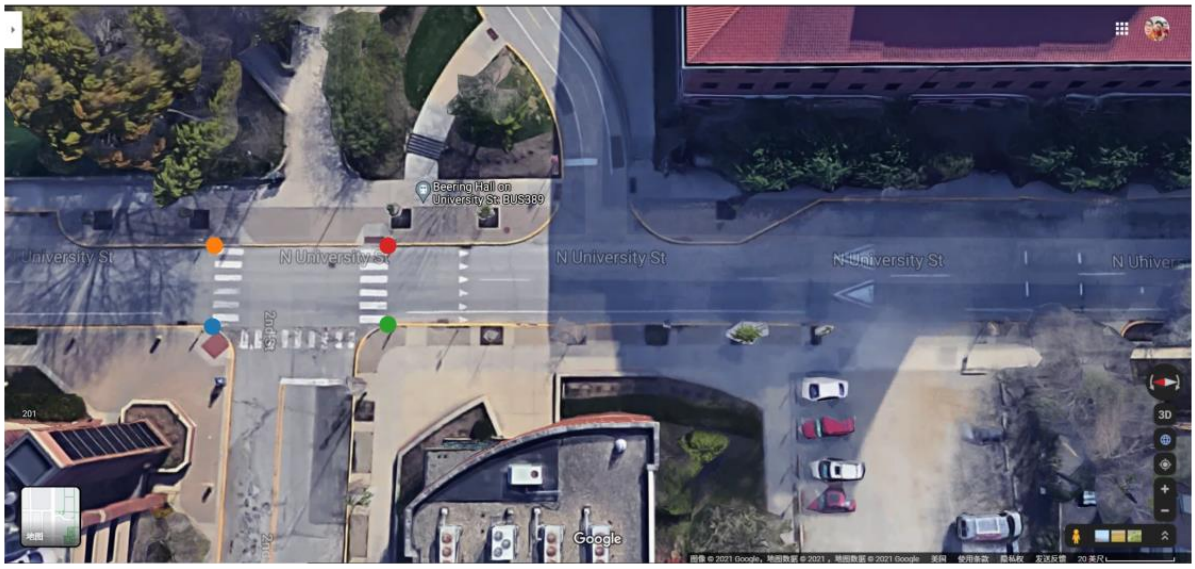

(b) Google Map View of the Study Site

Figure 6 Homography

The four colored points in Figure 6(a) can be projected onto the corresponding points in Figure 6(b) using the Homography matrix. Considering a two-dimensional point (x_1, y_1) in Figure

6(a) and the corresponding two-dimensional point (x_2, y_2) in Figure 6(b), a Homography is a transformation (a 3×3 matrix) that maps the (x_1, y_1) to the corresponding point (x_2, y_2) :

$$\begin{bmatrix} x_1 \\ y_1 \\ 1 \end{bmatrix} = H \begin{bmatrix} x_2 \\ y_2 \\ 1 \end{bmatrix} = \begin{bmatrix} h_{00} & h_{01} & h_{02} \\ h_{10} & h_{11} & h_{12} \\ h_{20} & h_{21} & h_{22} \end{bmatrix} \begin{bmatrix} x_2 \\ y_2 \\ 1 \end{bmatrix} \tag{1}$$

The Homography matrix *H* in Equation (1) can be estimated using the *findHomography* function in OpenCV (https://docs.opencv.org/3.4/d7/dff/tutorial_feature_homography.html). A script for the Homographic transformation of the given dataset can be found in our GitHub repository (https://github.com/YZhang-Genghis). The transformed pedestrian trajectories and vehicle trajectories are shown in Figure 7.

(a) Pedestrian Trajectories (b) Vehicle Trajectories

Figure 7 Transformed Road Users' Trajectories

3.1.3 Open-Sourced Trajectory Dataset

On-site cameras provided a bird's eye view of the intersection. The detection and tracking modules generate a large-scale spatial-temporal trajectory dataset from more than three hours of videos. The current dataset includes over 1 million frames/instances of spatial-temporal positions of heterogeneous road users (pedestrians, cyclists, and vehicles). More than 800 pedestrians and cyclists interacting with more than 500 vehicles are included.

1. This dataset will be larger than KITTI (Geiger et al., 2013) and ApolloScape (Ma et al., 2019), which have been widely used in trajectory predictions for heterogeneous road users.
2. The bird's eye view provides more interaction scenarios between heterogeneous road users (four PMIs in the Introduction) than BDD100K (Yu et al., 2018) and Argoverse (Chang et al., 2019) collected from naturalistic driving data.
    a. Naturalistic driving studies collect recordings of driving information from cameras inside multiple vehicles, which only provide interaction scenarios between the subject motorist and other road users (one-to-many). Our datasets provide many-to-many interaction scenarios.
    b. Recordings in naturalistic driving studies can only offer front-views and cannot provide adequate information about the surrounding environment.
3. Video recordings from another intersection are being processed by detection and tracking modules. After data cleaning, the dataset will be open-sourced. Moreover, Miovision cameras deployed at intersections in West Lafayette will be a perfect complement to the dataset.

Similar to the applications of KITTI, ApolloScape, BDD100K, and Argoverse, the open-sourced dataset can be used in planning, simulation, and prediction tasks. In Chapter 4 and Chapter 5, we will show how to use the trajectory dataset for prediction tasks. Simulation tasks are shown in Chapter 6.

3.2 PMI

A PMI is defined as the behavior of either party when in the area of influence of the other. Four examples of PMIs were offered in a previous study (Fricker and Zhang, 2019):

1. A pedestrian arrives at the curb and crosses immediately while a vehicle accelerates, slows down, or stops to avoid a conflict.
2. A pedestrian arrives at the curb and slows down or stops, but a vehicle slows down or stops to yield to the pedestrian.
3. A pedestrian arrives at the curb and slows down or stops, while a vehicle slows down, but does not yield to the pedestrian.

4. A pedestrian arrives at the curb and slows down or stops, while a vehicle keeps a constant speed or accelerates, not yielding to the pedestrian.

Once the analyst determines that one of the four cases occurred, a PMI will be recorded with explanatory variables in Table 2. Explanatory variables are extracted from the trajectory data. For example, at time *t*, if a PMI occurs, explanatory variables (d_{ped}, v_{ped}, d_{veh}, and v_{veh}) in Table 2 can be calculated via geospatial positions of the subject pedestrian and the interacted motorist at time *t* included in the trajectory profile. The variables (Gender and Group) can be determined by the analyst.

Table 2 Explanatory Variables

Variable	**Description**
V_{ped}	The approach speed (ft/s) of pedestrians when a pedestrian enters the curb area. Using Google Maps, the distance covered by a pedestrian every 34 milliseconds (one video frame) is converted into a speed. (mean = 3.34 ft/s; sd = 2.47 ft/s)
d_{veh}	The distance of interacted vehicle to the conflict point when the interaction begins (in feet). If an interaction occurs when the subject pedestrian arrives at the curb, we paused the video and calculated the distance to vehicle using Google Maps. (mean = 72.02 ft; sd = 54.14 ft) d_{veh} stands for the distance buffer of the vehicle.
d_{ped}	The direct distance of the subject pedestrian to the interacted vehicle when interaction begins (in feet). Let the pedestrian distance to the conflict point as $d_{conflict}$. $d_{ped} = \sqrt{d_{conflict}^2 + d_{veh}^2}$ (mean = 76.30 ft; sd = 51.72 ft). d_{ped} stands for the pedestrian's distance buffer.
Vveh	The approach speed (ft/s) of interacted vehicles when a pedestrian enters the curb area. Using Google Maps, the distance covered by a vehicle every 34 milliseconds (one video frame) is converted into a speed. (mean = 12.50 ft/s; sd = 10.29 ft/s)
Gender	A binary variable taking the value 1 if the subject pedestrian is a male (44.0%), 0 for female pedestrian (56.0%).
Group	The number of pedestrians in the subject pedestrian's curb area, including the subject pedestrian. (mean = 2.30; sd = 2.02)
Cross	A binary variable taking the value 1 if the pedestrian crosses; 0 otherwise.
P_{cross}	The interacted driver's belief that the pedestrian will cross.
Yield	A binary variable taking the value 1 if the driver yields; 0 otherwise
P_{yield}	The subject pedestrian's belief that the interacted driver will yield.
Note: mean = average value; sd = standard deviation	

The PMI events for this study were collected at two semi-controlled crossing locations on the Purdue University campus. See Figure 4(a) and Figure 4(b). We observed a total of 1607 PMIs.

At Intersection 1 – One-Way Grant St., we observed 170 PMIs in a 40-minute period (Time 1). At Intersection 2 – One-Way University St.,

a. Time 2: 8:30–9:20, with 123 interactions, 105 pedestrians and 125 vehicles observed;
b. Time 3: 13:25–14:00, with 271 interactions, 212 pedestrians and 152 vehicles observed;
c. Time 4: 16:20–17:00, with 386 interactions, 299 pedestrians and 170 vehicles observed; and
d. Time 5: 12:40–13:20, with 657 interactions, 517 pedestrians and 259 vehicles observed.

3.3 Data Collection at Signalized Crosswalks

We conducted a case study at the signalized crosswalk on Northwestern Avenue, leading to a parking garage at the Purdue University campus. See Figure 8 (a). The east-west street in Figure 8 is Northwestern Avenue. It has two 12-foot (3.66-meter) lanes in each direction, separated by a 12-foot (3.66-meter) raised median. The crosswalk is shown as the north-south "road" in Figure 8. We say "road", because that is how the crosswalk is represented in the Simulation of Urban MObility (SUMO) (Lopez et al., 2018), which is used in this study for microscopic traffic simulation. One important reason for choosing SUMO is that it is convenient to interface SUMO with Python.

Empirical data was collected by Boyu Cheng (Cheng, 2015). The detailed analysis of video recordings of more than 593 pedestrians and 611 vehicles at the Northwestern Garage crosswalk will be fed into the SUMO environment. Vehicle arrivals are assumed to follow a Poisson distribution with $\lambda = 0.08$/s (611 vehicles/2 lanes/3600 seconds), and pedestrian arrivals follow a Binomial distribution $B(5, 1/6)$ (1/6 = 593 pedestrians/3600 seconds). In this setting, pedestrian volume is moderate and vehicle volume is low.

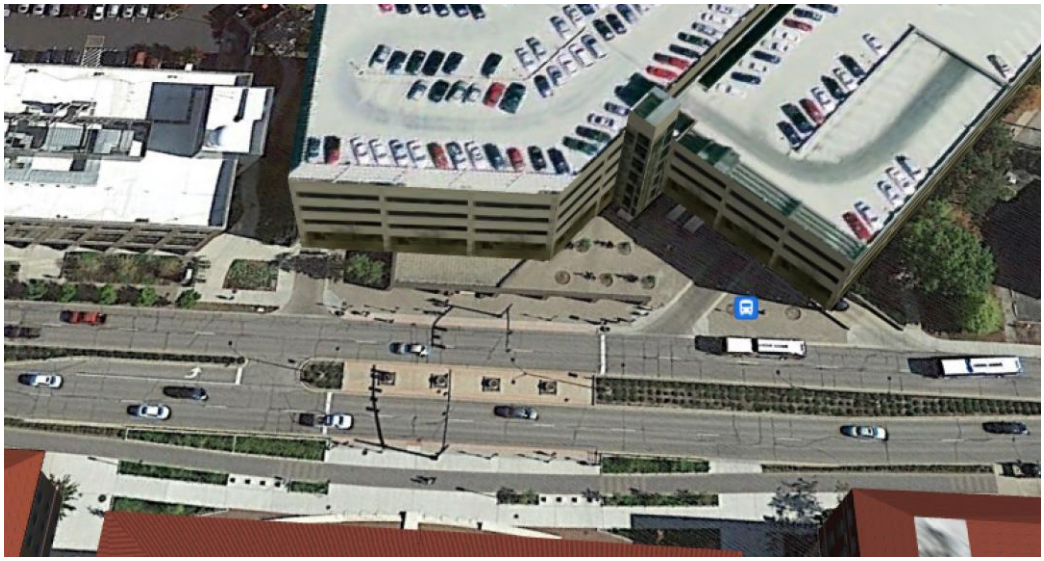

a. Google Earth View of Northwestern Garage Crosswalk

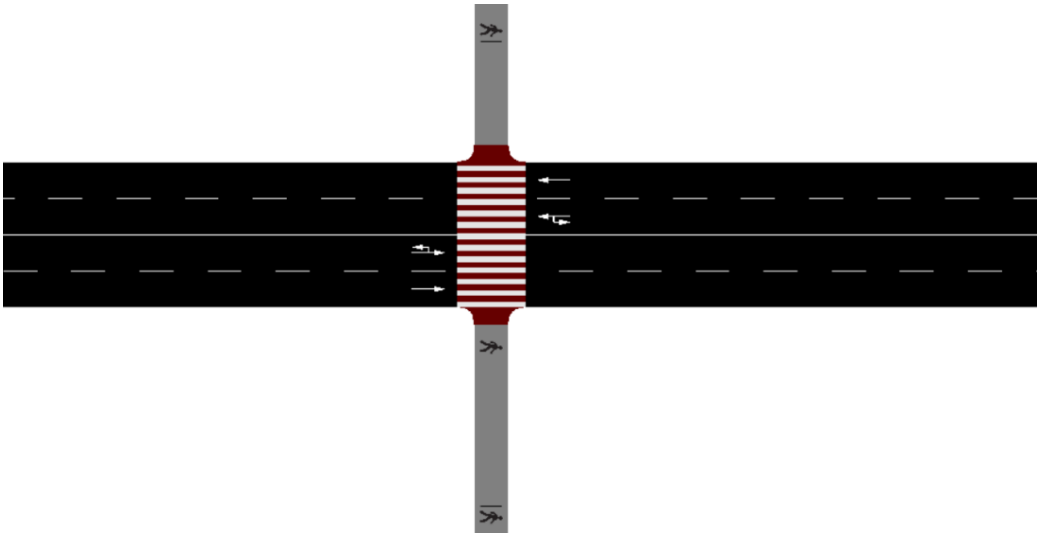

b. SUMO Representation of Northwestern Garage Crosswalk

Figure 8 Representations of Northwestern Avenue Crosswalk Environment

4. SAFETY AND EFFICIENCY ANALYSIS AT SEMI-CONTROLLED CROSSWALKS

This chapter is based on a published paper: Zhang, Y., & Fricker, J. D. (2021). Incorporating conflict risks in pedestrian-motorist interactions: A game-theoretical approach. *Accident Analysis & Prevention*, 159, 106254. This chapter tries to answer three key research questions:

1. How do we build the game between pedestrian and driver with incentives of time savings and conflict avoidance?
2. How do we reduce the probability of conflict between pedestrians and drivers at unsignalized crosswalks?
3. What is the relationship between the probability of conflict and the potential for crash occurrence?

4.1 Definitions

There are two types of pedestrian crossing decisions for each PMI:

- The subject pedestrian crosses immediately ($Y_p = 1$).
- The subject pedestrian waits and yields to the interacting motorist ($Y_p = 0$).

There are two types of driver yielding behavior for each PMI:

- The driver yields by stopping or slowing down ($Y_d = 1$).
- The driver doesn't yield to the pedestrian ($Y_d = 0$).

The joint behaviors of pedestrians and motorists can be represented as a payoff matrix, as shown in Table 3. The payoff matrix connects pedestrian crossing decisions with driver yielding decisions on the basis of "rewards".

1. If the payoff number is positive, the payoff is called a reward with a positive impact. For example,
    a. if the estimated payoff for {pedestrian crossing} and {driver yielding} is [2.74, 1.86]:

i. then the decision {pedestrian crossing} is associated with a reward of 2.74; and

ii. the decision {driver yielding} is associated with a reward of 1.86.

2. If the payoff number is negative, the payoff is called a cost with a negative impact.

   b. If the estimated payoff for {pedestrian crossing} and {driver not yielding} is [0, -1.072]:

      i. then the decision {pedestrian crossing} is associated with a reward of 0; and

      ii. the decision {driver not yielding} is associated with a negative reward of -1.072 (costs).

Initially, rewards are unknown (empty cells in Table 3) and can be estimated using PMI dataset.

In Table 3, two types of PMI are marked as safe and efficient:

1. PMI Case 1: The pedestrian crosses, and the driver yields (top-left cell).
2. PMI Case 2: The driver does not yield, and the pedestrian waits at the curb area (bottom-right cell).

There are two PMIs of special interest in Table 3:

3. PMI Case 3: The driver yields, and the pedestrian does not cross, which is called *confusion* (bottom-left cell).
4. PMI Case 4: The driver doesn't yield, and the pedestrian chooses to cross, which is called *conflict* (top-right cell).

Table 3 Initial Payoff Matrix

Payoff Matrix		Driver	
		Yield	No Yield
Pedestrian	Cross		
	Not Cross		

4.2 Model Formulation

The Quantal Response Equilibrium (QRE) builds on games with *incomplete information*. Such a game is formulated as: $G = \left\langle N,\ \{S_i\}_{i=1}^{N},\ \{A_i\}_{i=1}^{N},\ \{T_i\}_{i=1}^{N},\ P(t_1,...,t_T),\ \{u_i\}_{i=1}^{N} \right\rangle$,

1. The set of players N = {Pedestrian =1; Driver =2}.
2. The set of states S_t as described by explanatory variables in Table 2.
3. The set of actions for each player: pedestrian A_1 = {Cross; Not Cross} and driver A_2 = {Yield; Not Yield}.
4. The set of types for each player are: T_1 = {Aggressive; Cautious} given the state S_i:
    a. A pedestrian is considered aggressive if the pedestrian chooses the action {Cross};
    b. A pedestrian is considered cautious if the pedestrian does not cross.
    c. A driver is considered if the driver chooses the action {Yield}; and
    d. A driver is considered aggressive if the driver does not yield.
5. A joint probability distribution: P_t = {$P_{aggressive}$; $P_{cautious}$} over types, P_1 = {$P_{aggressive}$ = P_{cross}; $P_{cautious}$ = 1 – P_{cross}} and P_2 = {$P_{aggressive}$ = 1 – P_{yield}; $P_{cautious}$ = P_{yield}}.
6. The payoff matrix is represented as a combination of expected utility functions (payoff functions).

First, the state of nature of an interaction will determine the type of player that is measured by probability P_t. Then, the type of player determines the action that the subject player will choose with a probability.

- P_{yield} and P_{cross} are the parameters of the joint probability distribution.
- P_{yield} represents the pedestrian's belief that the interacted driver will yield. In other words, P_{yield} represents the pedestrian's belief that the interacted driver will be cautious.
- P_{cross} denotes the driver's anticipation that the subject pedestrian will cross. In other words, P_{cross} denotes the driver's anticipation that the subject pedestrian will be aggressive.
- The payoff matrix is represented as a combination of expected utility functions (payoff functions). Payoff functions are interrelated by players' actions and beliefs (P_{yield} and P_{cross}). See Equations 2b to 5b.

4.2.1 Expectation Utility Functions

Pedestrian Utility

Expectation utility functions for actions that the subject pedestrian may choose can be expressed as Equations 2a and 3a:

$$EU_{Cross} = p_{yield}(b_1 v_{ped}^2 + b_2 Gender + b_3 Group) \quad (2a)$$

$$EU_{Cross} = p_{yield} a_1 v_{ped}^2 \quad (2b)$$

$$EU_{DoNotCross} = b_4 d_{ped}^2 + b_5 d_{ped} + b_6 \quad (3a)$$

$$EU_{DoNotCross} = a_2 + a_3 d_{ped} \quad (3b)$$

Equations 2a and 3a become Equations 2b and 3b after eliminating variables that were found to be not statistically significant. If a pedestrian chooses to cross, the pedestrian will be motivated by reduced travel time but will undertake the risk of getting hit by a vehicle. P_{yield} represents the pedestrian's belief that the interacted driver will *yield*.

1. If the driver chooses to yield, then $P_{yield} = 1$, and the expected utility of crossing will be equivalent to $EU_{cross} = a_1 v_{ped}^2$, which denotes the benefits of saving time (positive rewards if a_1 is positive).
2. Otherwise, if the driver does not yield, then $P_{yield} = 0$, and the expected utility is equivalent to $EU_{Cross} = 0$, which represents the risk of a potential conflict (zero reward).

Driver Utility

Expectation utility functions for the actions that the interacted driver may choose are expressed as Equations 4a and 5a.

$$EU_{Yield} = b_7 d_{veh}^2 + b_8 d_{veh} + b_9 \quad (4a)$$

$$EU_{Yield} = a_4 d_{veh}^2 + a_5 d_{veh} + a_6 \quad (4b)$$

$$EU_{DoNotYield} = (1 - p_{cross})(b_{10} v_{veh}^2 + b_{11} v_{veh}) + b_{12} \quad (5a)$$

$$EU_{DoNotYield} = (1 - p_{cross})a_7 v_{veh}^2 + a_8 \quad (5b)$$

Equations 4a and 5a become Equations 4b and 5b after eliminating variables that were found to be not statistically significant. If a driver chooses not to yield, the driver will be motivated by reducing travel time but will assume the risk of hitting the pedestrian.

P_{cross} represents the driver's belief that the pedestrian will *cross*. If the pedestrian chooses to cross, then $P_{cross} = 1$, $1 - P_{cross} = 1 - 1 = 0$, and the expected utility of not yielding will (by Equation 4b) be equivalent to $EU_{\text{DoNotYield}} = a_8$, which represents the risk of a potential conflict for the driver (zero or negative reward).

If the pedestrian does not cross, then $P_{cross} = 0$, $1 - P_{cross} = 1 - 0 = 1$, and the expected utility (by Equation 5b) is equivalent to $EU_{\text{DoNotYield}} = a_7 v_{veh}^2 + a_8$, which denotes the benefit of saving time (positive rewards if $EU_{\text{DoNotYield}}$ is greater than zero).

4.2.2 Logit Quantal Response Equilibrium

A logit quantal response function is a particular class of quantal response function that has been widely used in the study of choice behavior. The logit quantal response function assumes that the players' anticipations are accurate on average, but subject to some errors that follow an extreme value distribution (McKelvey and Palfrey, 1995).

Equation 6 and Equation 7 take advantage of the expected utilities $\overline{EU}_{Cross}$, $\overline{EU}_{DoNotCross}$, $\overline{EU}_{Yield}$, and $\overline{EU}_{DoNotYield}$ to address the variability in the rewards across a population (Watling, 2006).

$$p_{cross} = \frac{\exp[\overline{EU}_{Cross}(p_{yield})]}{\exp[\overline{EU}_{cross}(p_{yield})] + \exp[\overline{EU}_{DoNotCross}]} \quad (6)$$

$$p_{yield} = \frac{\exp[\overline{EU}_{Yield}(1 - p_{cross})]}{\exp[\overline{EU}_{Yield}(1 - p_{cross})] + \exp[\overline{EU}_{DoNotYield}]} \quad (7)$$

Additionally, the players' anticipations P_{yield} and P_{cross} are determined by the logit quantal response functions in Equations 6 and 7.

- P_{cross} is the probability of the subject pedestrian choosing the strategy {*cross*} with the belief that the interacted driver will yield with the probability P_{yield}.
- P_{yield} is the probability of the interacted driver choosing the action {*yield*} with the anticipation that the subject pedestrian will cross with probability P_{cross}.

The existence and uniqueness of logit QRE has been asserted by McKelvey and Palfrey (1995). Mathematically, computing P_{yield} and P_{cross} is a fixed-point problem. P_{yield} and P_{cross} are fixed points of functions $P_{yield} = F(P_{cross})$ and $P_{cross} = H(P_{yield})$ (Brouwer, 1911).

Model parameters are estimated by maximum likelihood estimation. Let ΔEU_{Cross} and ΔEU_{Yield} be latent indices for pedestrian and motorist decisions:

$$\Delta EU_{Cross} = EU_{Cross} - EU_{DoNoCross} \tag{8}$$

$$\Delta EU_{Yield} = EU_{Yield} - EU_{DoNoYield} \tag{9}$$

The log-likelihood function of pedestrian decisions can be constructed:

$$LL_{ped}(a_1, a_2, a_3; y, X) = \sum_i \{\ln[\varphi(\Delta EU_{Cross})] * I\{y_i = 1\} + \ln[1 - \varphi(\Delta EU_{Cross})] * I\{y_i = 0\}\} \tag{10}$$

where,

- $y_i = 1$ represents that the subject pedestrian chooses the action {*cross*}.
- $y_i = 0$ represents that the subject pedestrian chooses the action {*not cross*}.
- $\varphi(.)$ is the cumulative distribution function of the logistic distribution.

Similarly, the log-likelihood function of driver decisions can be constructed:

$$LL_{veh}(a_4, a_5, a_6, a_7, a_8; y, X) = \sum_j \{\ln[\varphi(\Delta EU_{Yield})] * I\{y_j = 1\} + \ln[1 - \varphi(\Delta EU_{Yield})] * I\{y_j = 0\}\} \tag{11}$$

where

- $y_j = 1$ represents that the interacted driver chooses the action {*yield*}.
- $y_j = 0$ represents that the interacted driver chooses the action {*not yield*}.

Therefore, let μ denote the vector of all model parameters, and the log-likelihood can be expressed as:

$$LL(\mu; y, X) = LL_{ped}(a_1, a_2, a_3; y, X) + LL_{veh}(a_4, a_5, a_6, a_7, a_8; y, X) \tag{12}$$

4.2.3 Solution Algorithm - Expectation Maximization

Expectation Maximization (EM) can be applied iteratively to generate solutions for logit QRE. P_{yield} and P_{cross} can be considered latent variables. For a pair of initial probabilities {$P_{cross,i}$, $P_{yield,i}$}, μ_i is generated by maximizing the total log-likelihood function (Dixit and Denant-Boemont, 2014):

$$\begin{aligned} \max_{\mu_i} LL(\mu_i; y, X) = {} & LL_{ped}(a_1, a_2, a_3; y, X, P_{yield,i}) + \\ & LL_{veh}(a_4, a_5, a_6, a_7, a_8; y, X, P_{cross,i}) \end{aligned} \tag{13}$$

For μ_i, a new pair of probabilities {$P_{cross,i+1}$, $P_{yield,i+1}$}is generated based on Equation 14 and Equation 15:

$$p_{cross,i+1} = \frac{\exp[\overline{EU}_{Cross}(p_{yield,i}, \mu_i)]}{\exp[\overline{EU}_{Cross}(p_{yield,i}, \mu_i)] + \exp[\overline{EU}_{DoNotCross}(\mu_i)]} \tag{14}$$

$$p_{yield,i+1} = \frac{\exp[\overline{EU}_{Yield}(1 - p_{cross,i}, \mu_i)]}{\exp[\overline{EU}_{Yield}(1 - p_{cross,i+1}, \mu_i)] + \exp[\overline{EU}_{DoNotYield}, \mu_i]} \tag{15}$$

Equations 13-15 can be applied iteratively until {$P_{cross,i}$, $P_{yield,i}$} converges. The pseudocode of the proposed EM algorithm is shown in Figure 9.

Algorithm 1 Expectation Maximization

Initialization $\leftarrow \epsilon$, $v = 0$, $P_{0,cross}$, $P_{0,yield}$.

$\mu = \{a_1, a_2, a_3, a_4, a_5, a_6, a_7, a_8\}$.

while $P_{v,cross} - H(P_{v,yield}) > \epsilon$ Or $P_{v,yield} - F(P_{v,cross}) > \epsilon$ **do**

$LL(\mu; y, X, P_{v,cross}, P_{v,yield}) = LL_{ped}(a_1, a_2, a_3; y, X, P_{v,yield}) + L_{veh}(a_4, a_5, a_6, a_7, a_8, P_{v,cross})$

$\mu_{v+1} \in \arg\min LL(\mu; y, X, P_{v,cross}, P_{v,yield})$

$P_{v+1,cross} = H(P_{v,yield}; \mu_{v+1})$

$P_{v+1,yield} = F(P_{v,cross}; \mu_{v+1})$

$v = v + 1$

end

Figure 9 Expectation Maximization Algorithm

The convergence of the EM algorithm has been shown by Wu (1983). The logit QRE usually converges within 150 iterations. Traceplots (see Figure 10) of P_{cross} and P_{yield} with 150 iterations are utilized to show the convergence of the logit QRE. P_{cross} and P_{yield} converge to 0. 0.848 and 0.475, respectively.

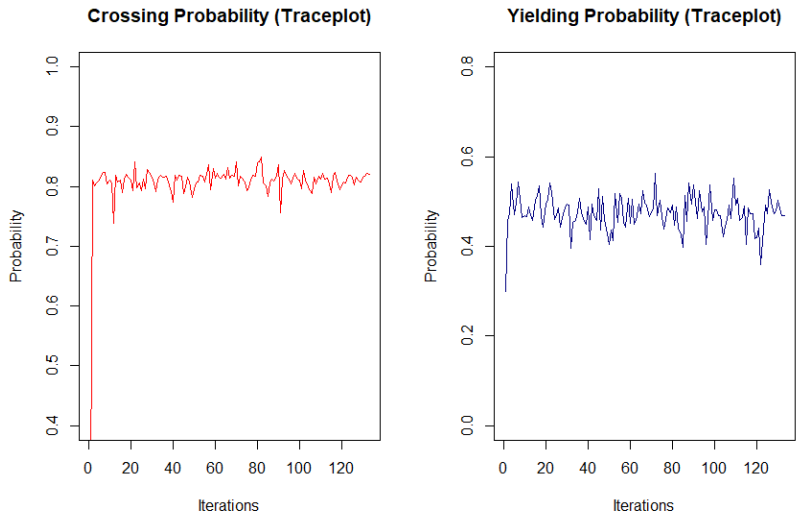

Figure 10 Traceplots of Fixed-Point Iteration

4.3 Estimation Results

The estimation results are shown in Table 4. Parameters and variables used in Equations 2b, 3b, 4b, and 5b are shown in the first column of Table 4. "Bootstrap standard deviation" is a surrogate estimate of standard error (Train, 2009). The z-score is an indication of how far from zero an estimated coefficient is. If the absolute value of a z-score is greater than 1.96, we can conclude that the estimated parameter is "significant" at the 95 percent confidence level. Note that a_6 represents the intercept in Equation 5b. Including the intercept will make the model more flexible, even if the intercept is not significant.

Table 4 Estimation Results for Model Parameters

Parameter and Variable	Coefficient	Bootstrap Standard Deviation	z_score	$P > \|z\|$
a_1 V_{ped}^2	0.245	0.043	5.654	0.000
a_2	1.920	0.513	3.746	0.000
a_3 d_{ped}	-0.024	0.005	-4.682	0.000
a_4 d_{veh}	0.054	0.023	2.389	0.017
a_5 d_{ped}^2	-0.00030	0.00013	-2.382	0.017
a_6	-0.464	0.593	-0.782	0.434
a_7 V_{veh}^2	0.057	0.010	5.484	0.000
a_8	-1.072	0.506	-2.119	0.034

4.3.1 Pedestrian Dynamics

Parameter a_1 is associated with the approach speed (ft/s) of a pedestrian when he/she enters the curb area. A positive a_1 represents the increase in the probability of a pedestrian crossing if the pedestrian approaches the curb with a higher velocity. The pedestrian approach speed has a strong correlation with the probability of {Cross} decision of the subject pedestrian. See Equation 2b.

4.3.2 Vehicle Dynamics

Similarly, the estimation for parameter a_6 is associated with the approach speed (ft/s) of a driver when a PMI occurs. A positive a_6 represents the increase in the probability of a driver not yielding if the vehicle approaches the crosswalk at a higher speed.

4.3.3 Pedestrian Distance to Conflict Point

The estimation parameters $a_2 = 1.92$ and $a_3 = -0.024$ are related to the pedestrian's action – {*not cross*}. A negative a_3 represents the decrease in the probability of a pedestrian not crossing if the direct distance between the subject pedestrian and the interacted vehicle is higher.

4.3.4 Vehicle Remaining Distance

d_{veh} also reveals a non-linear effect on a driver's decision. If the distance to the conflict point is less than 89.49 ft, the expected utility function for {*yield*} increases with the increase in distance to the conflict point. Therefore, the probability of {*yield*} increases.

When $d_{veh} > 89.49$ ft, the expected utility function for {*yield*} decreases as d_{veh} increases. There are two possible explanations.

1. A driver may observe the pedestrian's behavior first and then respond to it because there's an adequate buffer for the driver to "think about" the best action.
2. There may be no need for the driver to yield because, if the pedestrian leaves the curb area quickly and crosses quickly, the driver will not have to yield (as defined in Table 2).

4.4 Payoff Matrix

The payoff matrix can be derived by applying the estimated coefficients in Table 4. Each entry in Table 5 represents the payoff from each action. Each player will choose an action to maximize the payoff.

If the mean values of explanatory variables are used in the payoff functions, the entries in the last two rows of Table 5 result. Each entry represents the expected utility or payoff of each action. In game theory, a *strictly dominant* strategy is defined as one that always provides greater utility than another strategy for one player. When a vehicle approaches the crosswalk at the speed of 5 ft/s, the payoff for {not yield} is $0.057 * 5^2 - 1.072 = 0.353$, and the payoff for {yield} is no less than 0.353 if d_{veh} lies in the range [16.7, 163.3] by solving the equation. The dominant strategy will be {yield} for the driver. Dominant strategy is a key point in the perfect Nash equilibrium

game, assuming perfect rationality for every player. In the Quantal Response Equilibrium, perfect rationality is relaxed to the bounded rationality, and either a dominant or dominated strategy can be chosen in a probability.

Table 5 Payoff Matrix

		Driver	
		Yield	Do Not Yield
Pedestrian	Cross	$[0.245v_{ped}^2,$ $0.054d_{veh} - 0.0003d_{veh}^2 - 0.464]$	[0, -1.072]
	Do Not Cross	$[1.92 - 0.024d_{ped},$ $0.054d_{veh} - 0.0003d_{veh}^2 - 0.464]$	$[1.92 - 0.024d_{ped},$ $0.057v_{veh}^2 - 1.072]$
Pedestrian (mean case)	Cross	[2.74, 1.86]	[0, -1.072]
	Do Not Cross	[1.49, 1.86]	[1.49, 7.84]

It is clear in the "mean value" case that there is no strictly dominant strategy for both pedestrians and drivers. For example, if the pedestrian chooses the action {*cross*}, the potential outcome is 2.74 when the interacted motorist chooses to *yield*, or 0 when the interacted motorist chooses *not to yield*. If the pedestrian chooses the action {*not cross*}, the potential outcome is always 1.49. The outcomes for the action {*cross*} are not always greater than the outcomes for the action {*not cross*}. This demonstrates that the best pedestrian strategy depends on the driver's behavior (the probability of the driver yielding as perceived by the pedestrian). Neither pedestrian behavior is dominant. In the absence of a dominant strategy, a player must decide on an action based on the expected action of the other player. The uncertainties in this zebra crossing game raise issues of safety and efficiency. Of special interest are the probabilities of the two special cases of interactions:

- *Confusion*: the driver yields, and the pedestrian does not cross.
- *Conflict*: the driver doesn't yield, and the pedestrian chooses to cross.

4.5 Safety and Efficiency Analysis

We define the probabilities of conflict and confusion as:

$$p_{conflict} = p_{cross} * (1 - p_{Yield}) \tag{16}$$

$$P_{confusion} = (1 - P_{Cross}) * P_{yield} \quad (17)$$

$P_{conflict}$ and $P_{confusion}$ are two important performance measures. $P_{conflict}$ is the probability that a conflict occurs, representing the conflict risk. $P_{confusion}$ is the probability that a misunderstanding between a pedestrian and a motorist happens, which is an efficiency measure at the semi-controlled crosswalk.

4.5.1 Conflict and Confusion Prediction

Sample calculations of the probability of conflict and the probability of confusion are provided for a pedestrian-motorist interaction (PMI) with covariate values of d_{ped} = 51.80 ft, d_{veh} = 38.97 ft, v_{ped} = 3.69 ft/s, and v_{veh} = 28.24 ft/s.

1. Set initial parameters for the first step in the algorithm (Figure 9). Here, P_{cross} = 0.7, P_{yield} = 0.4, and ε = 0.001 are chosen.
2. Calculate the expected utilities. Equations 18-21 below are Equations 2b-5b for the sample calculations:

$$EU_{Cross} = 0.4 * 0.245 * 3.69^2 = 1.334 \quad (18)$$

$$EU_{DoNotCross} = 1.92 - 0.024 * 51.80 = 0.677 \quad (19)$$

$$EU_{Yield} = 0.054 * 38.97 - 0.0003 * 38.97^2 - 0.464 = 1.185 \quad (20)$$

$$EU_{DoNotYield} = (1 - 0.7) * 28.24^2 - 1.072 = 12.565 \quad (21)$$

3. Recalculate the probabilities using Equations 6 and 7: P'_{cross} = 0.659 and $P'_{yield} = 1.142 * 10^{-5}$.
4. Stop if the convergence requirement is met, viz., $P'_{cross} - P_{cross} < \varepsilon$ and $P'_{yield} - P'_{yield} < \varepsilon$. Else, $P_{cross} = P'_{cross}$, $P_{yield} = P'_{yield}$, and repeat Steps 1-3.
5. At convergence, P_{cross} = 0.309 and $P_{yield} = 2.224 * 10^{-13}$.
6. Calculate the probability of conflict as $P_{conflict} = 0.309 * (1 - 2.224 * 10^{-13}) = 0.309$ and the probability of confusion as $P_{confusion} = (1 - 0.309) * 2.224 * 10^{-13} = 1.538 * 10^{-13}$.

The high value of $P_{conflict}$ reflects the low distance (38.97 ft) of the vehicle to the conflict point, a high vehicle approach speed (28.24 ft/s), and a moderate pedestrian approach speed (3.69 ft/s).

4.5.2 Relationship between Explanatory Variables and Conflict

An essential research question will be: how to reduce the probability of conflict between pedestrians and drivers at semi-controlled crosswalks? Based on Equations 16 and 17, the relationship between the explanatory variables and the probability of conflict $P_{conflict}$ is indirect. For example, the coefficient a_6 is associated with the approach speed (ft/s) of a driver when a PMI occurs. A change in vehicle approach speed will directly influence the probability of vehicle yielding P_{yield} as perceived by the pedestrian. A change in P_{yield} will result in a change in the probability of pedestrian crossing P_{cross}. The probability of conflict is derived as $P_{conflict} = P_{cross} * (1 - P_{yield})$, which is Equation 16. According to Equations 2b and 5b, the change in vehicle approach speed will result in changes in both P_{yield} and P_{cross}. Hence, the relationship between the explanatory variables and the probability of conflict is not direct.

For this reason, a sensitivity analysis was conducted by predicting changes in conflict probability if there was a 10% change in any one of the variables listed in Table 2, holding constant the values of all other variables. The sensitivity analysis is based on the following five steps:

1. For each pedestrian-motorist interaction (PMI), calculate the probability of conflict ($P_{conflict}$) and confusion ($P_{confusion}$) based on the six-step conflict prediction in Section 4.5.1, given the observed values of d_{ped}, d_{veh}, v_{ped}, and v_{veh} for the PMI. The green bars in Figure 11(a) comprise the frequency histogram after $P_{conflict}$ has been calculated for all PMIs.
2. Change by 10% the value of a given predictor variable for each PMI and calculate the new probability of conflict $P'_{conflict}$ and probability of confusion $P'_{confusion}$, based on Equations 16 and 17. The red bars in Figure 11(b) represent the frequency distribution of the probability of conflict $P'_{conflict}$ for all PMIs, given a 10% increase in the original value of V_{veh} for each PMI.
3. Calculate $P'_{conflict} - P_{conflict}$ for the current PMI and add the result to the frequency distribution of changes in conflict probability for V_{veh}.

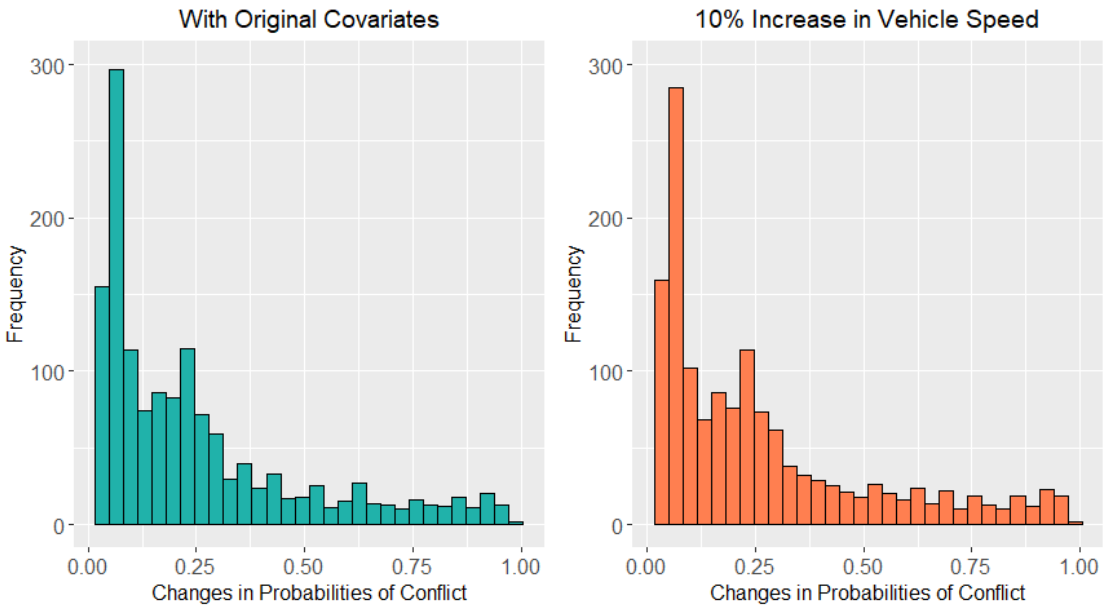

(a) (b)

Figure 11 Distributions of Conflict Probability Before-and-After

4. After all PMIs have been examined, draw the histogram for the frequency distribution of changes in conflict probability for V_{veh}. See Figure 12(a).
5. Repeat Steps 1-4 for the other explanatory variables and build histograms, as shown in Figure 12(b), Figure 12(c), and Figure 12(d).

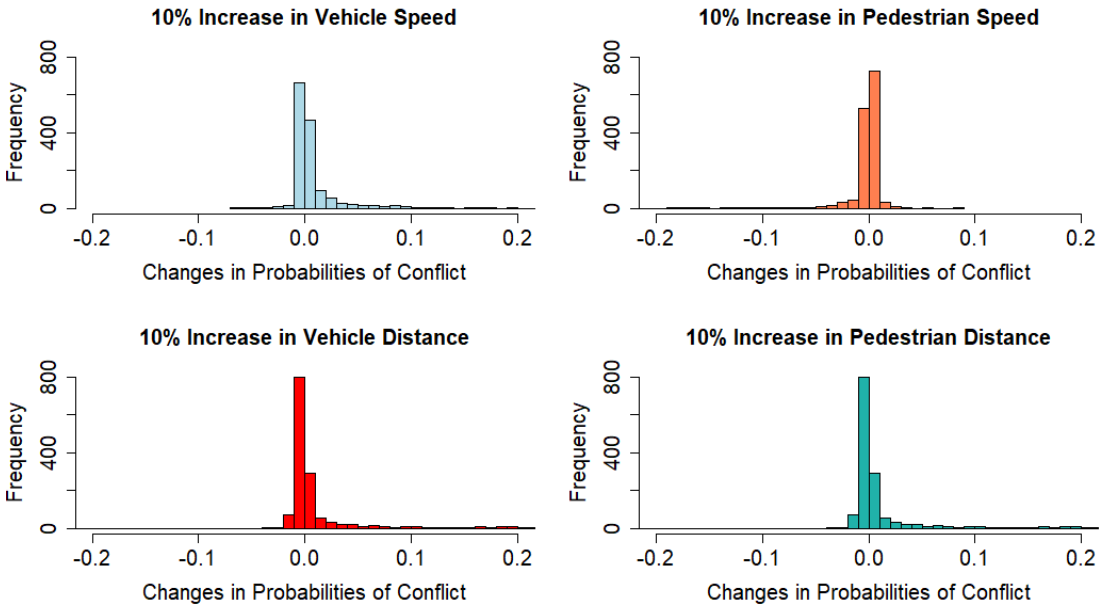

Figure 12 Sensitivity Analysis

The histograms in Figure 12 indicate that an increase in an explanatory variable will not necessarily lead to an expected change in the probability of conflict. For example,

- Based on Equations 5b and 7, an increase in the vehicle approach speed (V_{veh}) will result in a lower probability of yield P_{yield}.
- A decrease in P_{yield} will also result in a reduction of P_{cross}, based on Equations 2b and 6.
- However, an increase in $(1 - P_{yield})$ and the decrease of P_{cross} will not necessarily lead to a reduction in the probability of conflict, as calculated by Equation 16.

When we compare the top two histograms in Figure 12 to the bottom two histograms, it is apparent that Probabilities of conflict are more sensitive to changes in distances than to changes in speeds. If the vehicle distance to the conflict point is increased by 10%, $P_{conflict}$ is usually reduced, by as much as 0.01 in some cases. Perhaps surprisingly, the $P_{conflict}$ response to a 10% increase in vehicle approach speed is very small, usually between -0.1 and +0.2. In response to changes in

pedestrian approach speed and pedestrian distance to the conflict point, changes in $P_{conflict}$ will be larger for the distance, but without positive or negative tendencies in either case.

These results may provide clues to control measures at the crosswalk. Controlling vehicle approach speed is possible, but it will not necessarily reduce conflict probabilities, based on the results of the game theory analysis. The findings with respect to vehicle distance to the conflict point may inform the design of traffic control at the crosswalk or whether new controls at the semi-controlled crosswalk should be implemented at all. In the next section, we mainly discuss the effectiveness of controlling vehicle distance to the conflict point.

4.5.3 Relationship between Vehicle Distance to the Conflict Point and Conflict

The bottom left histogram in Figure 12 indicates that an increase in vehicle distance to the conflict point (d_{veh}) will result in a lower probability of conflict. For a zebra crossing game, the three scenarios identified in a previous paper (Zhang et al., 2020) are used:

1. If a vehicle is too close to yield to the subject pedestrian ($d_{veh} \leq 30$ ft), the normal pedestrian choice is to "let the vehicle go first", and it will cause little delay for the pedestrian.
2. If a vehicle is too far away ($d_{veh} > 120$ ft), the normal pedestrian choice is to cross without any hesitation, because the pedestrian will feel safe.
3. If the vehicle is neither too far from the crosswalk nor too close (esp. 40 ft to 50 ft, as demonstrated in (Zhang et al., 2020), the zebra crossing game will be more complicated and more instructive. We set a range for the parameter ($30 \text{ ft} < d_{veh} \leq 80$ ft) in Scenario 3.
4. The remaining range for the parameter ($80 \text{ ft} < d_{veh} \leq 120$ ft) is set in Scenario 4.

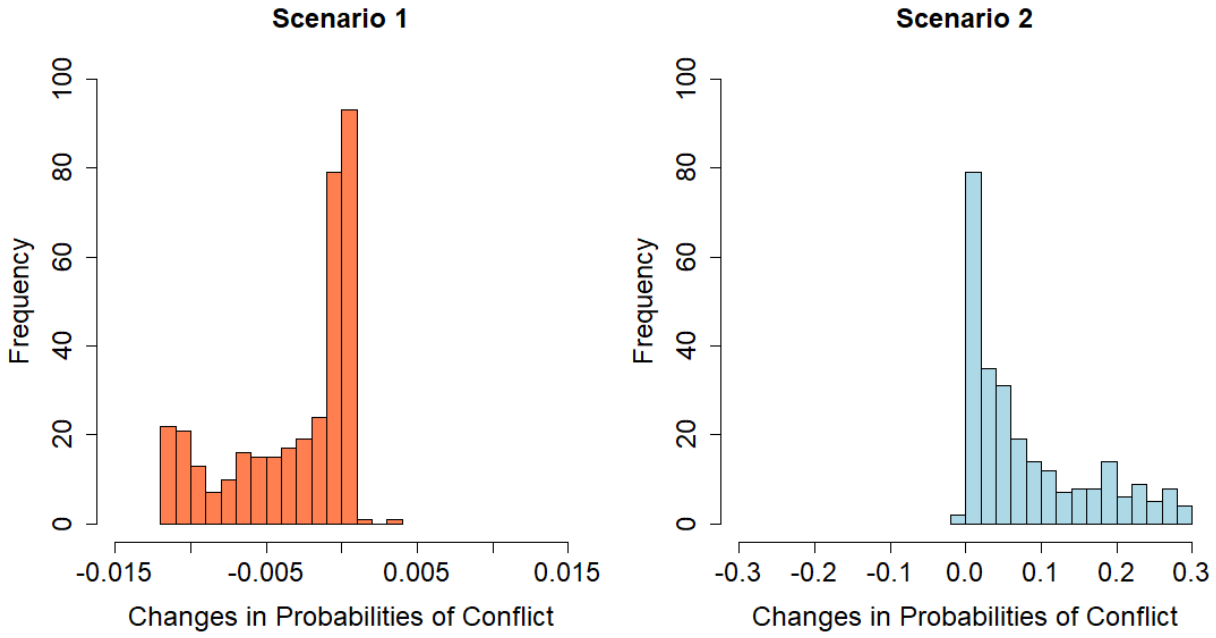

(a) (b)

Figure 13 Changes in Conflict Probabilities under Scenario 1 and Scenario 2

The first and second scenarios will not involve dangerous situations. If a vehicle is too close to the subject pedestrian, a 10% increase in distance is a small change (e.g., 20 feet versus 22 feet). Sensitivity analysis for only the Scenario 1 observations in the database (d_{veh} < 30 ft) indicates minor changes in the probability of conflict (-0.015 to 0.005) that are based on Equation 4b. See Figure 13(a).

If a vehicle is "too far away", a 10% increase in distance will result in larger changes in d_{veh} (e.g., 200 feet versus 220 feet). Sensitivity analysis for only the Scenario 2 observations in the database (d_{veh} >120 ft) indicates major changes in the probability of conflict (0 to 0.3). If a vehicle is too far away (d_{veh} >120 ft), the normal pedestrian choice is to cross without any hesitation, because the pedestrian will feel safe. Therefore, a 10% increase in the vehicle distance to the conflict point will have little effect.

However, in the third scenario (30 ft < d_{veh} ≤80 ft), a large proportion of pedestrians must quickly consider the costs of being hit and the costs of delay. If at least one player has incorrect expectations concerning the behavior of the others, such inefficient communication can lead to

unsafe situations. The results of the sensitivity analysis are shown in Figure 14(a). An increased vehicle distance to the conflict point usually reduces the probability of conflict in Scenario 3.

An increased vehicle distance to the conflict point usually *increases* the probability of conflict in Scenario 4 (80 ft < d_{veh} ≤ 120 ft). As we discussed in Section 4.3.4, when d_{veh} > 89.49 ft, the expected utility function for {*yield*} decreases as d_{veh} increases. There are two possible explanations. (1) A driver may observe the pedestrian's behavior first and then respond to it because there's an adequate buffer for the driver to "think about" the best action. (2) There may be no need for the driver to yield because, if the pedestrian leaves the curb area quickly and crosses quickly, the driver will not have to yield. See Figure 14(b).

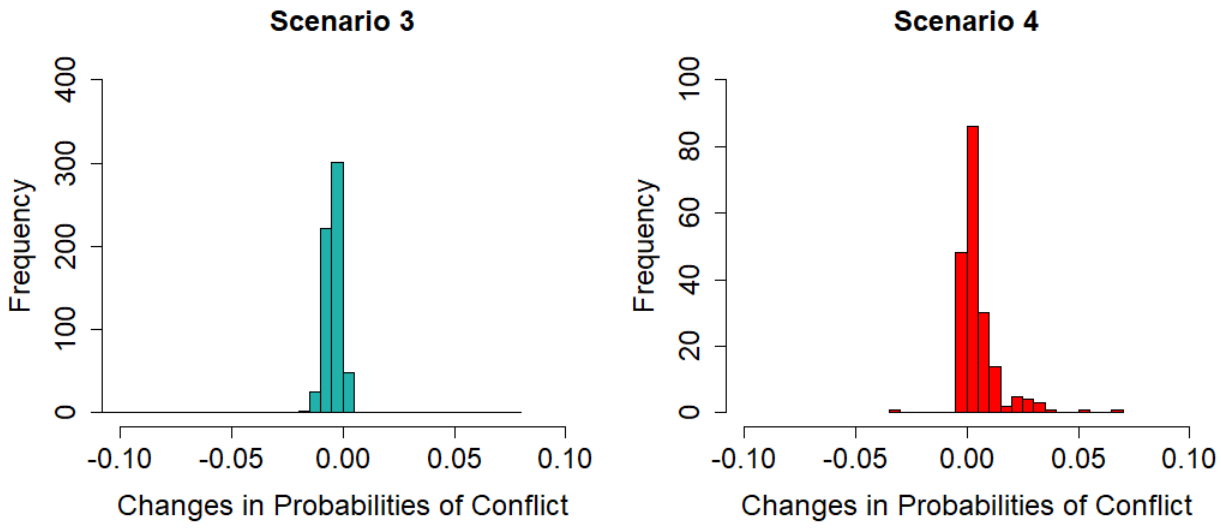

(a) (b)

Figure 14 Changes in Conflict Probabilities under Scenario 3 and Scenario 4

4.6 Surrogate Measure of Crash - Probability of Conflict

In the previous section, the probability of conflict was proposed as a safety measure at semi-controlled crosswalks. A robust safety measure should be consistent with crash potential. Therefore, this section examines the relationship between the probability of conflict and the driver

yielding rate, which is a commonly used measure of crash potential at unsignalized crosswalks (Fu et al., 2018).

4.6.1 Intersection 3 - Two-Way University St.

Data collection was conducted at two intersections with five different time periods. By the time additional videos were made in Spring 2018, the one-way University St. had been converted to a two-way operation. After the conversion, the street is 34 feet wide, with two 5-foot bicycle lanes and a speed limit of 25 mph. The two sets of video recordings were made at three different time periods (7:40-8:40; 12:00-13:00; and 16:20-17:20), when low-to-moderate traffic volumes and pedestrian flows could be observed:

a. Time 6: 16:20-17:20 with 554 PMIs observed;
b. Time 7: 7:40-8:40 with 318 PMIs observed; and
c. Time 8: 12:00-13:00 with 652 PMIs observed.

The dataset for this study was collected at **three** semi-controlled crossing locations on the Purdue University campus. In total, we observed 3133 pedestrian-motorist interactions (PMIs). The estimation results and payoff matrices (similar to Table 4 and Table 5) are shown in the Appendix. The estimation results are consistent among three different semi-controlled crosswalks.

4.6.2 Validity of Probability of Conflict

We collected data from **three** different semi-controlled crossing locations in **eight** different time periods, during which there are temporal variations in traffic volumes and pedestrian flows. These **three** datasets were separated into **eight** subsets based on the time period when we collected the data. The validity of the probability of conflict is based on the following four steps:

1. Driver yielding rates for the **eight** datasets are calculated as:
    a. Derive the number of PMIs with Yield = 1 (from Table 2) at dataset *i* as $N_{yield,\ i}$.
    b. Derive the total number of PMIs at the dataset *i* as $N_{total,\ i}$.
    c. Derive the driver yielding rate for dataset *i* as $p_{yield} = \frac{N_{yield,\ i}}{N_{total,\ i}}$.
2. Conflict probabilities of conflicts on average for the **eight** datasets are derived via the proposed six-step method.

3. A linear regression (R^2 = 0.71) has been developed in Figure 15 to delineate the relationship between observed driver yielding rates (x-axis) and calculated conflict probabilities (y-axis).
4. A negative relationship (y = 0.499 – 0.431x) between calculated conflict probabilities and observed driver yielding rates has been found, which indicates that an increase in the driver yielding rate will result in a lower calculated conflict probability.

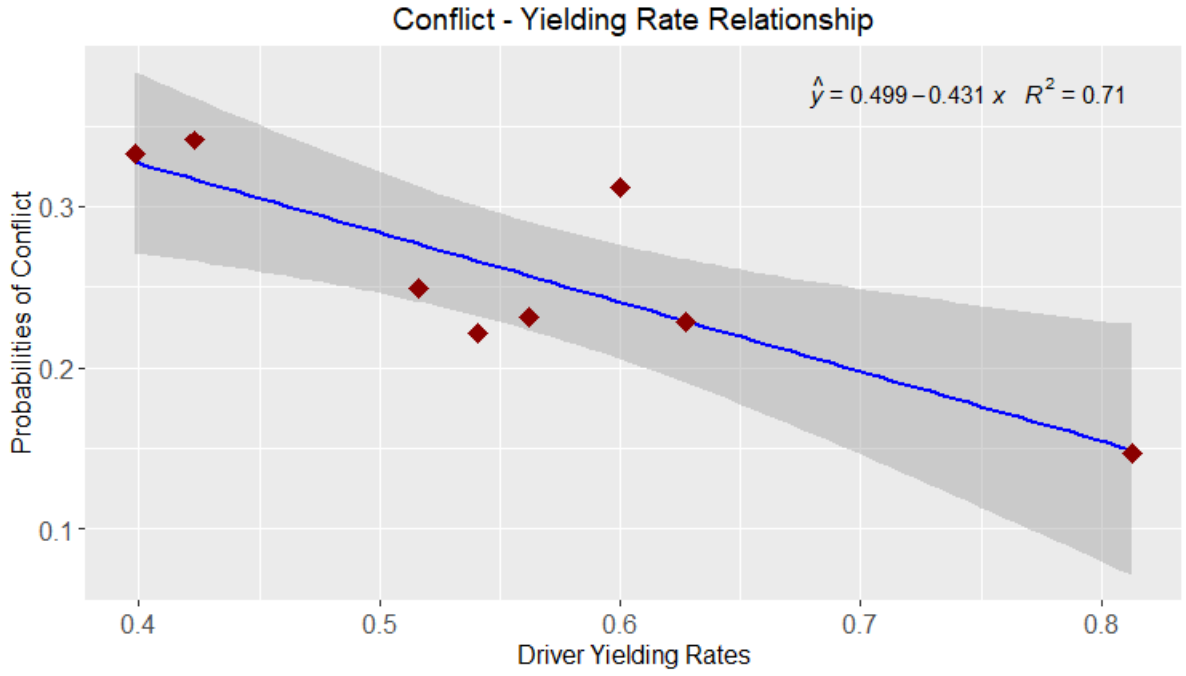

Figure 15 Relationship Between Probability of Conflict and Driver Yielding Rate

4.7 Model Comparisons

As documented by hours of video, the assertion of priority results from a silent "negotiation" between pedestrian and driver. Patterns of behavior emerged. Statistically significant factors are being identified, while variations in behavior are also being recognized. Behavioral models were built from the pedestrian point of view and the driver point of view in our previous studies:

1. Mixed logit models were used to model pedestrian crossing behavior, and generalized ordered logit regression was applied to model driver deceleration behavior (Fricker and Zhang, 2019; Zhang, 2019).

2. Multi-State Semi-Markov models were utilized to model pedestrian waiting behavior (Zhang et al., 2020) and driver waiting behavior (Zhang and Fricker, 2020).

The family of logit models and multi-state Semi-Markov models estimated pedestrian and driver behavior separately in previous studies. However, the zebra-crossing game models joint behavior (Equations 2b to 5b) that connects pedestrians' actions (P_{cross}) with drivers' decisions (P_{yield}), which is the key difference between previous studies and the zebra-crossing game.

Multi-State Semi-Markov models were applied for survival analysis with time-to-event data instead of PMI data. Multi-State Semi-Markov models were omitted, and logistic regression was chosen as the baseline. To compare the game-theoretic approach with the baseline in previous studies, the model accuracy, which is measured by five-fold cross validation in Table 6, is used as a metric. The general procedure for cross-validation is:

1. The complete dataset is randomly shuffled and separated into five groups.
2. For each unique group:
    a. Take the group as a test dataset and the remaining groups as a training dataset.
    b. Fit a model on the training data and evaluate it on the test data:
        i. The zebra-crossing game is fitted using Equations 2 to 15. Parameters are derived (like the parameters in Table 4). Model parameters are then used to evaluate the test set.
        ii. Logistic regression is trained twice:
            - One logistic regression is to model pedestrian crossing behavior using the predictors in Equations 2a and 3a.
            - The other is to model driver yielding behavior using the predictors in Equations 4a and 5a.
    c. Model parameters are then used to evaluate the test set.
3. Report the prediction accuracy of the test dataset.

The higher the accuracy, the better the model performance is. The bold values in Table 6 indicate better model accuracies. The zebra-crossing game has better accuracies in seven out of ten trials in Table 6.

Table 6 Model Comparisons in Five-Fold Cross Validation

	Folds	Decision	Zebra-Crossing Game	Logistic Regression
Cross-Validation	**1**	Pedestrian	83.33%	**84.70%**
		Driver	**80.56%**	77.40%
	2	Pedestrian	**87.50%**	85.00%
		Driver	80.10%	**82.20%**
	3	Pedestrian	**89.50%**	87.10%
		Driver	**79.40%**	74.90%
	4	Pedestrian	**85.40%**	**85.40%**
		Driver	76.30%	**77.70%**
	5	Pedestrian	**87.80%**	86.50%
		Driver	**78.50%**	78.10%

4.8 Discussion

Recall the three research questions proposed at the beginning of this chapter:

1. Question 1 has been answered in Sections 4.2 and 4.3.
2. Question 2 has been answered in Sections 4.4 and 4.5.
3. Question 3 has been answered in Section 4.6.

4.8.1 Contributions

Three research questions have been answered, but how does this study help inform the design of control measures (if any) at the crosswalk? Because Figure 12 shows us that $P_{conflict}$ is sensitive only to d_{veh}, increasing d_{veh} from the current value for each PMI covered by Scenario 3 will do the most to reduce $P_{conflict}$ and improve safety. Three strategies suggest themselves:

1. First, determine if a need for a control measure exists. The value of $P_{conflict}$ generated by the methods in this paper can serve as a guide in that respect. For example, if too many PMIs fall above a certain value of $P_{conflict}$ (say, 0.15) in Figure 11(a), control measures may be justified.
2. Although active controls might be considered, it may be sufficient (and even preferable) to install passive controls such as speed humps at a distance from the crosswalk that

reduces $P_{conflict}$ to an acceptable level. The findings of this study are consistent with a distance of 40 feet to 50 feett that was demonstrated by Zhang et al. (2020).

3. A real-time conflict risk assessment framework can be developed using the predicted $P_{conflict}$. Prediction results ($P_{conflict}$) can be shared with heterogeneous road users to avoid potential collisions.

4.8.2 Study Scope and Limitations

This study investigated the "zebra crossing" game involving two players – pedestrians and motorists – at semi-controlled crosswalks. 1607 pedestrian-motorist interactions were observed, and the joint behavior of driver and pedestrian as they interact in real street-crossing situations was explored. As more data is gathered in our dataset, the model can be further updated, and the model performance is expected to be better. In addition, there are several limitations in the model-based game:

1. Limit information in data: the data used in the model was collected by a single analyst. The event-based framework only includes information about a PMI at one time stamp when the PMI occurs. As a remedy, pedestrian and vehicle trajectory data containing information over multiple time steps will be utilized in the next chapter.
2. Restricted model: expected utility functions are fixed in the pre-specified model. Agents are unlikely to behave exactly in the way that the model-based game describes. Advanced computational models will be explored in the next chapter.

5. FORECASTING MOTIONS OF HETEROGENEOUS ROAD USERS AT SEMI-CONTROLLED CROSSWALKS

This chapter is based on a paper submitted to a conference: *Zhang, Y., Fricker, J. (2022). "Forecasting the Motion and Behavior of Heterogeneous Road Users at Crosswalks: A Spatial Temporal Graph-Based LSTM Approach". Submitted to IEEE International Conference on Robotics and Automation.*

The objective of this chapter is to propose a model to predict the future trajectories of heterogeneous road users by considering their observed trajectories and interactions. The proposed model is an extension of the zebra-crossing game, as mentioned in Section 1.2 and Section 4.8.2.

5.1 Motion Prediction

The motion prediction problem is to estimate the future trajectories (from time t+1 to time t_f) of road users who appear at the time stamp t, based on their observed trajectories (from time t-t_h+1 to time t) and interactions.

5.1.1 Trajectory

The definition of the trajectory for the subject road user i can be formulated as a time sequence: $Tr_i\left(x_t, y_t\right) \in \{\mathfrak{R}^2\}$, where $\left(x_t, y_t\right) \in \mathfrak{R}^2$ represents the spatial coordinates of the subject road user's position at time t.

5.1.2 Input – Observed Trajectory

The input of the model is the observed trajectory of the subject road user i over t_h time steps (t_h = 3 seconds): $X_i\left(Ob\_Tr_i\right) = \left[\left(x^{(i)}_{t-t_h+1}, y^{(i)}_{t-t_h+1}\right), \left(x^{(i)}_{t-t_h+2}, y^{(i)}_{t-t_h+2}\right), \ldots, \left(x^{(i)}_{t}, y^{(i)}_{t}\right)\right]$.

5.1.3 Prediction – Future Trajectory

The output of the model is the future trajectory of the subject road user i over t_f time steps (t_f = 3 seconds): $Y_i\left(Fut\_Tr_i\right) = \left[\left(x_{t+1}^{(i)}, y_{t+1}^{(i)}\right), \left(x_{t+2}^{(i)}, y_{t+2}^{(i)}\right), \ldots, \left(x_{t+t_f}^{(i)}, y_{t+t_f}^{(i)}\right)\right]$.

5.2 Network Architecture

The Spatial-Temporal Graph-Based Seq2Seq model structure is shown in Figure 16.

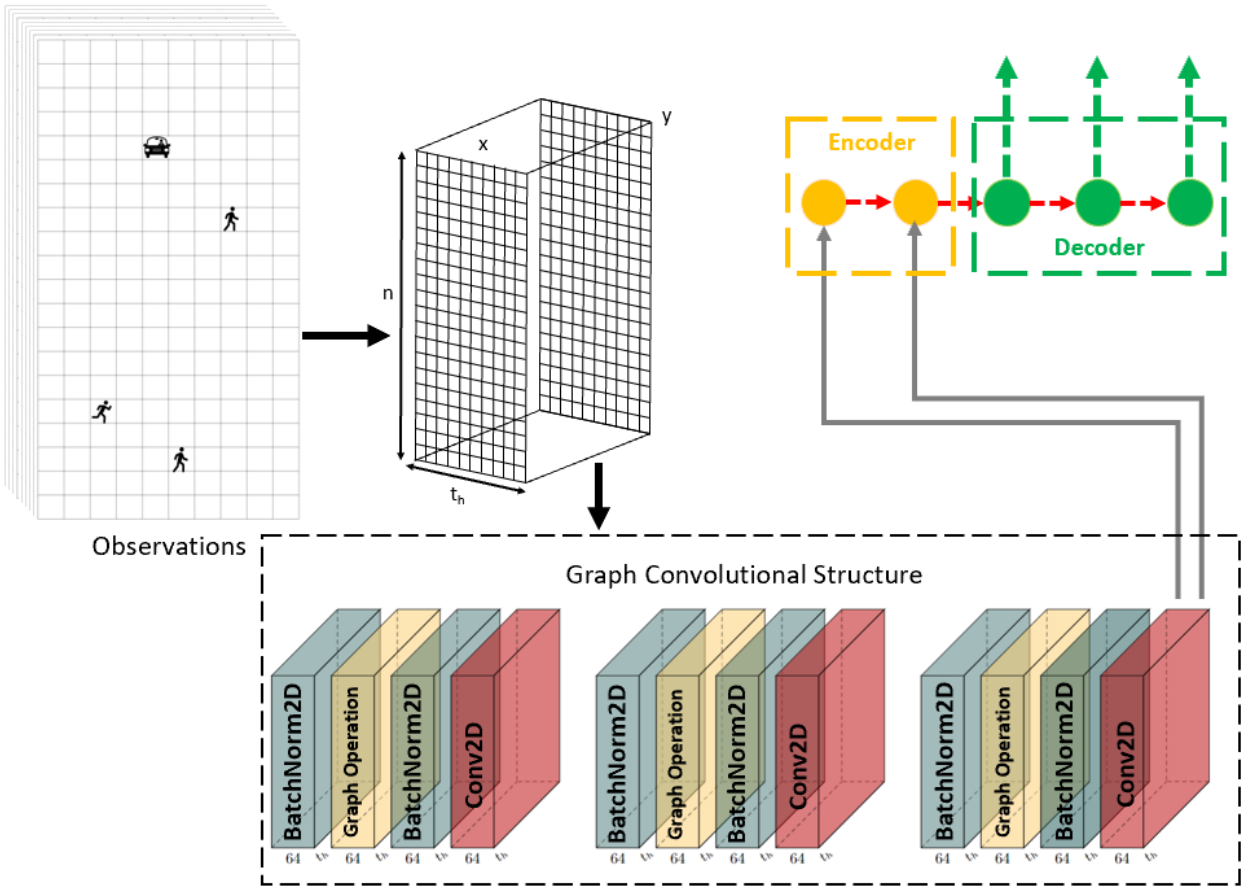

Figure 16 Spatial-Temporal Graph-Based Seq2Seq Model Structure

5.2.1 Input

The dataset can be represented as $t \times C \times P \times V$:

- t represents the total number of time frames.

- C represents the number of features (category of road users, longitudinal coordinate, latitudinal coordinate, and heading direction).
- $P = t_h + t_f$ represents the temporal domain with observed 3-second and predicted 3-second frames.
- $V = 20$ represents the maximum number of road users shown in one frame. The value of V can change based on the types of data.

The entire dataset is split into subsets (mini batches). Each mini batch can be represented as a tensor with a size of ($n \times C \times t_h \times V$), where n represents the number of mini-batches, C represents the vector of 2-dimensional spatial coordinates $\left(x_t, y_t \right) \in \mathfrak{R}^2$ and additional features such as the category of road users and head direction, t_h represents the number of observed time frames, and $V = 20$ represents the maximum number of road users showing in one frame. See Figure 16.

5.2.2 Spatial-Temporal Graph Construction

In urban traffic settings, subject road users' movements are significantly influenced by nearby agents (see the four PMI cases mentioned in the Introduction). To handle the interdependencies between the trajectory of the subject road user and the trajectories of surrounding road users, we propose a social network graph – an undirected graph $G = \{V, E\}$, where the nodes (V) represent road users and the edges (E) represent interactions between road users.

- Each node v_{it} in the node set V, represents a road user i appearing in a time frame t. Then, the node set can be constructed as $V = \left\{ v_{it} \mid i = 1, \ldots, n;\ t = 1, \ldots, t_h \right\}$.
  - n is the total number of road users observed at a time frame t; and
  - the feature vector ($F\left(v_{i,t}\right)$) of the node v_{it} consists of the spatial coordinates $\left(x_t^{(i)}, y_t^{(i)} \right)$ of the road user i at a time t.
- The edge set E consists of two parts:
  - $E_S = \left\{ \left(v_{it}, v_{jt} \right) \mid Dist\left(i, j\right) \le D \right\}$: the set of edges that describe the spatial interactions between node v_{it} and node v_{jt}.

- $Dist(i, j)$ represents the Euclidean distance between the road user *i* and the road user *j*.
- *D* is a threshold value that represents the spatial closeness between the road user *i* and the road user *j* in one frame. In this dissertation, we first choose a large *D* value, as *D* = 380 feet (116 meters).
  - If the spatial distance between node v_{it} and node v_{it} is less than *D* at time *t*, the pair of nodes (v_{it}, v_{jt}) is included in the edge set E_S.
  - A large *D* value represents that every pair of - nodes (v_{it}, v_{jt}) shown in the same time frame *t* will be included in the edge set E_S regardless of the spatial distance between road user *i* and road user *j*.

- $E_T = \{(v_{it}, v_{i(t+1)})\}$: the set of edges that describe the temporal difference only for the road user *i* between time *t* and *t*+1. All pairs of edges in E_T for road user *i* represent the trajectory of road user *i*.

- To better demonstrate the interaction between road users at a single frame *t*, an adjacency matrix $A = [I, A_s]$ is proposed:
  - I indicates the self-connection of the subject road user in temporal space; and
  - A_S indicates whether any pair of nodes (v_{it}, v_{jt}) is in the edge set E_S :

$$A_S[i][j] = \begin{cases} 1 & \text{if } (v_{it}, v_{jt}) \in E_S \\ 0 & \text{otherwise} \end{cases} \quad (22)$$

  - Both I and A_S are $n \times n$ square matrices, where *n* is equal to the number of road users appearing in each time frame.

5.2.3 Spatial Temporal Graph Convolutional Network (ST-GCN) Module

The graph convolutional module (Yan et al., 2018) consists of three parts:

1. BatchNorm2D: batch normalization is a technique for training deep neural networks that standardizes the inputs to a layer for each mini-batch (Ioffe and Szegedy, 2015). For each input ($n \times C \times t_h \times V$), BatchNorm2D operation normalizes the input using Equation (23).

$$y = \frac{X - E[X]}{Var[X] + \varepsilon} \times \gamma + \beta \tag{23}$$

where:

- ε is a value added to the denominator for numerical stability to avoid a denominator of zero.
- γ, β are learnable parameter vectors of size C.
- The Batch Normalization is done over the C dimension, computing statistics on (n, t_h, V) slices.

2. Graph operations: these are known as layer-wise propagations across graph convolutional networks (GCN). Layers of GCN are proposed to capture the spatial interactions of all road users appearing at time t. Layer-wise propagations across GCN can be implemented with the following equation (Kipf and Welling 2016):

$$f_{g,\,out} = \sigma\left(D^{-\frac{1}{2}} A D^{-\frac{1}{2}} f_{g,\,in} W\right) \tag{24}$$

where:

- $A = A_S + I$ is the adjacency matrix we defined in the Spatial-Temporal Graph Construction section.
- $D^{ii} = \sum_j A_{ij} + \alpha$, D represents the degree matrix of A (Kipf and Welling, 2016), and $\alpha = 0.001$ is a small number to avoid empty rows in A_{ij}.
- $\sigma(.)$ denotes the activation function, such as $ReLU(.) = max(0, .)$.
- W denotes the layer-specific learnable weight matrix.

3. Conv2D: Temporal convolutional (TCN) layers are proposed to capture the temporal dependencies between consecutive spatial positions of a road user. The output of a GCN layer ($f_{g,\,out}$) is normalized by one BatchNorm2D layer and fed into the TCN layer as $f_{t,\,in}$. A kernel with a size of 1 × 5 is applied to each 2-D convolutional layer with

appropriate paddings and strides to move along the temporal axis (t_h) shown in Figure 16. For an input of $f_{t,\,in}$, the output of each TCN layer can be represented as $f_{t,\,out}$.

5.2.4 Seq2Seq

The graph convolutional module is followed by the Seq2Seq module. The Seq2Seq framework is an encoder-decoder network.

The encoder takes the sequence of output of graph convolutional module (length of t_h) - $O_{t'} = \left[O_{t-t_h+1}, O_{t-t_h+2}, \ldots, O_{t-1}, O_t\right]$, feeds it to the embedding layer, derives the series of hidden states $h_{t'} = \left[h_{t-t_h+1}, h_{t-t_h+2}, \ldots, h_{t-1}, h_t\right]$ (for example, a Gated Recurrent Unit (GRU) encoder will calculate the hidden states as h_t = EncoderGRU($e(O_t)$, h_{t-1}), where e denotes the embedding operation), and generates the context vector $z = h_t$. The context vector z will be fed to the decoder for future trajectory predictions.

The decoder first calculates the series of hidden states $s_{t'} = \left[s_{t+1}, s_{t+2}, \ldots, s_{t+t_f-1}, s_{t+t_h}\right]$. For example, a GRU decoder will calculate the hidden states as s_t = DecoderGRU($d(y_t)$, s_{t-1}, z). The target value for the next time stamp is calculated as $y_{t+1} = f(d(y_t), s_t, z)$, where f is a linear layer.

Recall that the prediction $Y_i(Fut\_Tr_i) = \left[\left(x_{t+1}^{(i)}, y_{t+1}^{(i)}\right), \left(x_{t+2}^{(i)}, y_{t+2}^{(i)}\right), \ldots, \left(x_{t+t_f}^{(i)}, y_{t+t_f}^{(i)}\right)\right]$ represents the future spatial coordinates of the subject road user's position over t_f time steps. At each time step, the decoder is to predict the two-dimensional spatial coordinate - $\left(x_{t+i}, y_{t+i}\right) \in \Re^2$ where $i \in \left[1,\ t_f\right]$. The predicted coordinate (x or y) is activated by a *tanh* function within the scale (-1, 1), which will be further re-scaled into real coordinates.

5.3 Implementation Details

ST-GCN shares the same weights (weight matrix W in Equation 24) on different nodes. It is important to keep the scale of the input data consistent. In this study, we normalize the spatial coordinates within the range of (-1, 1). The ST-GCN-Seq2Seq model is composed of 3 units of

ST-GCN. All three ST-GCN units have 64 channels for output. We randomly dropout the features with a probability of 0.5 in each ST-GCN unit to avoid overfitting.

Smooth L1 Loss is chosen as the criterion. For a batch size of *N*, smooth L1 loss can be represented as:

$$l(R,P) = L = \{l_1, l_2, \ldots, l_N\}^T$$

$$l_n = \begin{cases} 0.5(R_n - P_n)^2 / beta & if\ |R_n - P_n| < beta \\ |R_n - P_n| - 0.5 \times beta & otherwise \end{cases} \quad (25)$$

$$l(R,P) = mean(L) \quad (26)$$

beta = 1, is chosen as the default parameter.

Adam (Kingma and Ba, 2014) is used as the optimization algorithm to train the model with a learning rate of 0.01. The learning rate decays by 0.1 every 10 iterations.

5.4 Experiment and Results

5.4.1 Evaluation Metrics

The root mean squared error (RMSE) of predicted trajectories in the future (3-second horizons) will be reported. The RMSE can be calculated as:

$$RMSE = \sqrt{\frac{1}{N} \times \frac{1}{T} \times \frac{1}{t_f} \sum_{i=1}^{N} \sum_{t=1}^{T} \sum_{k=1}^{t_f} \left(x_{t+k}^{(i)} - \hat{x}_{t+k}^{(i)}\right)^2 + \left(y_{t+k}^{(i)} - \hat{y}_{t+k}^{(i)}\right)^2} \quad (27)$$

where,

$x_{t+k}^{(i)}$ denotes the real longitudinal coordinate of road user *i* at time *t*+*k*.

$\hat{x}_{t+k}^{(i)}$ denotes the predicted longitudinal coordinate of road user *i* at time *t*+*k*.

$y_{t+k}^{(i)}$ denotes the real latitudinal coordinate of road user *i* at time *t*+*k*.

$\hat{y}_{t+k}^{(i)}$ denotes the predicted latitudinal coordinate of road user *i* at time *t*+*k*.

5.4.2 Comparison Methods

To test model performance, we compared the proposed model with state-of-the-art (SOTA) models. The SOTA models were chosen based on two metrics:

1. The SOTA method should be applicable to pedestrian, cyclist, or vehicle motion predictions.
2. The SOTA method should be open-access and have been evaluated or validated by other studies.

Accordingly, five SOTA models were chosen as baselines:

1. The Social-Force (SF) model is a physics-based model developed by Helbing and Molnar (1995). It is widely used to simulate pedestrian dynamics in an urban traffic environment.
2. The Convolutional Social Pooling (ConvSP) (Deo et al., 2018) adopted a convolutional social pooling mechanism in the LSTM encoder-decoder model, addressing vehicle-vehicle interactions using the Next Generation Simulation (NGSIM) datasets. A visualization of the proposed ConvSP- LSTM is shown in Figure 17.
3. The Social-LSTM has the same model structure as the ConvSP-LSTM model except for the convolutional social pooling module (Alahi et al., 2016). Instead, a fully connected pooling (FCSP) module has been adopted to address interactions between road users. The difference between ConvSP and FCSP is similar to the difference between the Convolutional Neural Network (CNN) and fully connected neural networks in image recognition (LeCun and Bengio, 1995).
4. Seq2Seq is a classical sequence-to-sequence model that has been widely applied in the area of natural language processing. The LSTM Encoder-Decoder can be considered the same model as the ConvSP-LSTM model without the convolutional social pooling module.

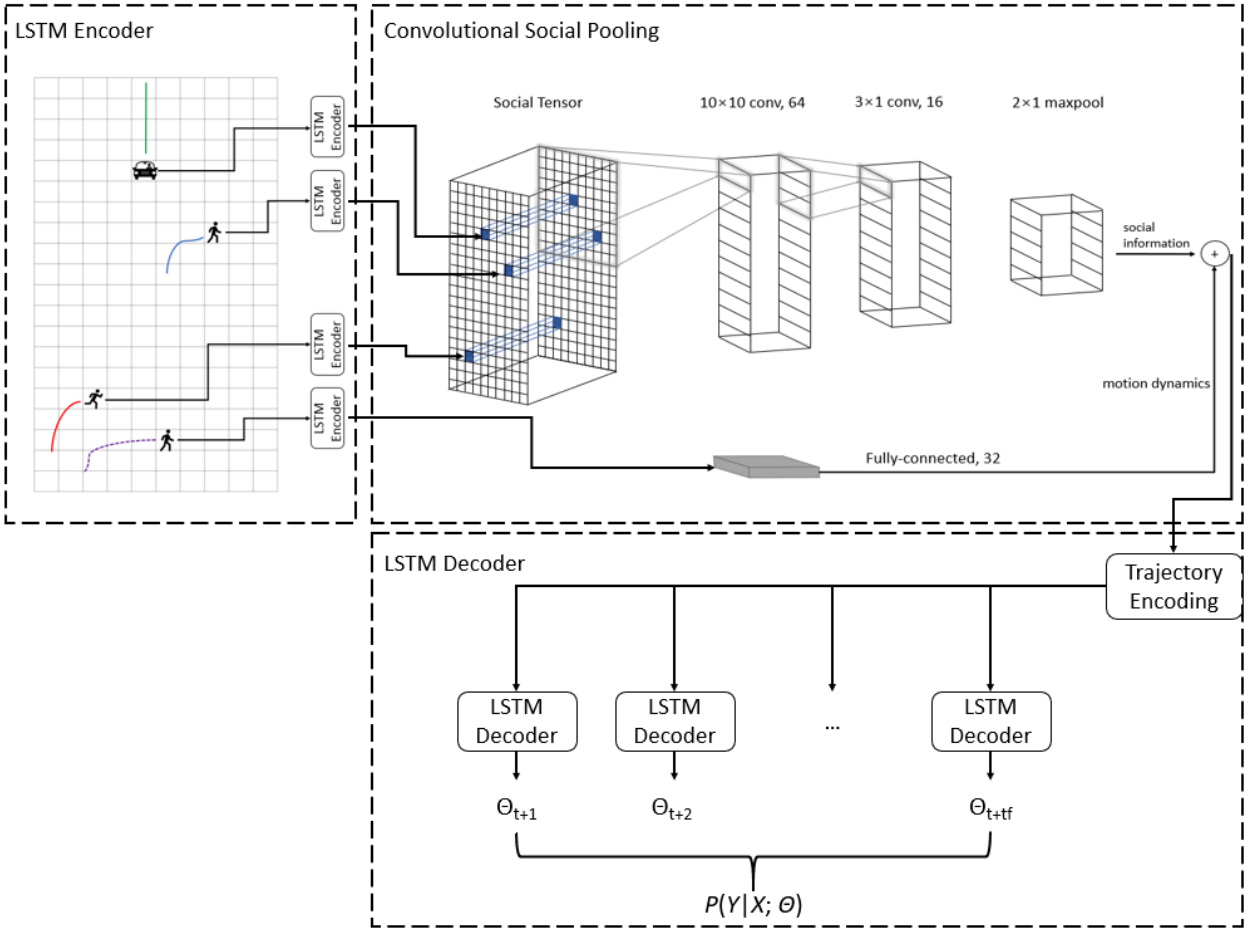

Figure 17 ConvSP-LSTM Structure

5.4.3 Modifications on SOTA

It is worth noting that all the SOTA models predict the motions of homogenous road users based on observed trajectories and their interactions. These SOTA models adopt different strategies to encode interactions between homogenous road users. To better implement the SOTA models, we slightly modified the mechanism in the SOTA models, considering interactions between heterogeneous road users. We slightly modified these models to account for interactions between heterogeneous road users, which does not necessarily reflect the original intent of these models.

For example, when we modified the ConvSP-LSTM model, a larger ConvSP layer was required due to the complicated pedestrian-motorist interactions (Fricker and Zhang et al., 2019). We define the area of influence as a series of grid cells – 20 (90 meters) × 10 (40 meters) to be the area of influence. Each grid cell has a height of 4.5 meters and a width of 4 meters. A visualization of the ConvSP is shown in Figure 17.

- The first convolutional kernel for the social tensor is 10 × 10. The size of the first output (C_1) is 11 × 1 × 64.
- The second convolutional kernel for C_1 is 3 × 1. The size of the second output (C_2) is 9 × 1 × 16.
- A 2 × 1 max-pooling operation with padding (1, 0) is conducted after C_2, resulting in a 5 × 1 × 16 final output (C_3) for the social information of the subject road user.
- C_3 is concatenated with the encoded motion dynamics of the subject road user as the trajectory encoding in Figure 17.
- Finally, the trajectory encoding will be sent to the LSTM decoder to predict future trajectories of the subject road user.

Social-LSTM has a similar structure where the convolutional social pooling module is replaced by a fully connected pooling module (Alahi et al., 2016). The Seq2Seq model only consists of the LSTM Encoder and the LSTM decoder modules shown in Figure 17. The supplementary materials for the proposed methods and the SOTA models can be found in our GitHub repository (https://github.com/YZhang-Genghis).

5.4.4 Model Results

The complete dataset is separated into training and validation sets. The validation set contains the last 20% of trajectories in the dataset. RMSE values are reported in the validation set. All units are in meters. The lower the MSE values, the better the model performance is. The bold values in Table 7 indicate the best model performance.

Table 7 Model Comparisons

Evaluation Metric	Prediction Horizon (s)	SF	Seq2Seq	Social-LSTM	ConvSP-LSTM	ST-GCN-Seq2Seq
RMSE (m)	0.5	0.406	0.672	0.256	0.267	**0.196**
	1	0.661	1.082	0.322	0.343	**0.234**
	1.5	0.783	1.287	0.359	0.385	**0.272**
	2	1.022	1.704	0.447	0.481	**0.341**
	2.5	1.140	1.916	0.498	0.538	**0.377**
	3	1.371	2.348	0.638	0.706	**0.452**

It is worth noting that the SF model is used for pedestrian trajectory prediction only because it is widely used for pedestrian simulation. The SF model has rarely been used in the simulation of vehicle motions. In addition, the accuracy of pedestrian trajectory predictions is higher than vehicle trajectory predictions (less RMSE) by the other models. Consequently, it is reasonable to conclude that the SF model results are not as good as ST-GCN-Seq2Seq.

5.5 Case Studies

Note that we conduct case studies based on the validation set of data.

5.5.1 Pedestrian-Vehicle Interaction Scenario

Figure 18 shows the trajectory prediction results considering the vehicle-vehicle interaction. Recall that there is a stop sign on 2nd St., which means that vehicles on 2nd St. have to stop before the stop line. As shown in Figure 18, the blue solid lines indicate the ground truth future trajectories (3s) for pedestrians and vehicles, and the red dashed lines represent the predicted future trajectories (3s) for pedestrians and vehicles.

1. The subject pedestrian saw a vehicle approaching and jaywalked without stopping in the curb area because, if the subject vehicle is too far away, the normal pedestrian decision is to cross immediately.
2. The subject vehicle was keeping a constant speed. The driver did not have to slow down or stop to avoid a conflict with the subject pedestrian.

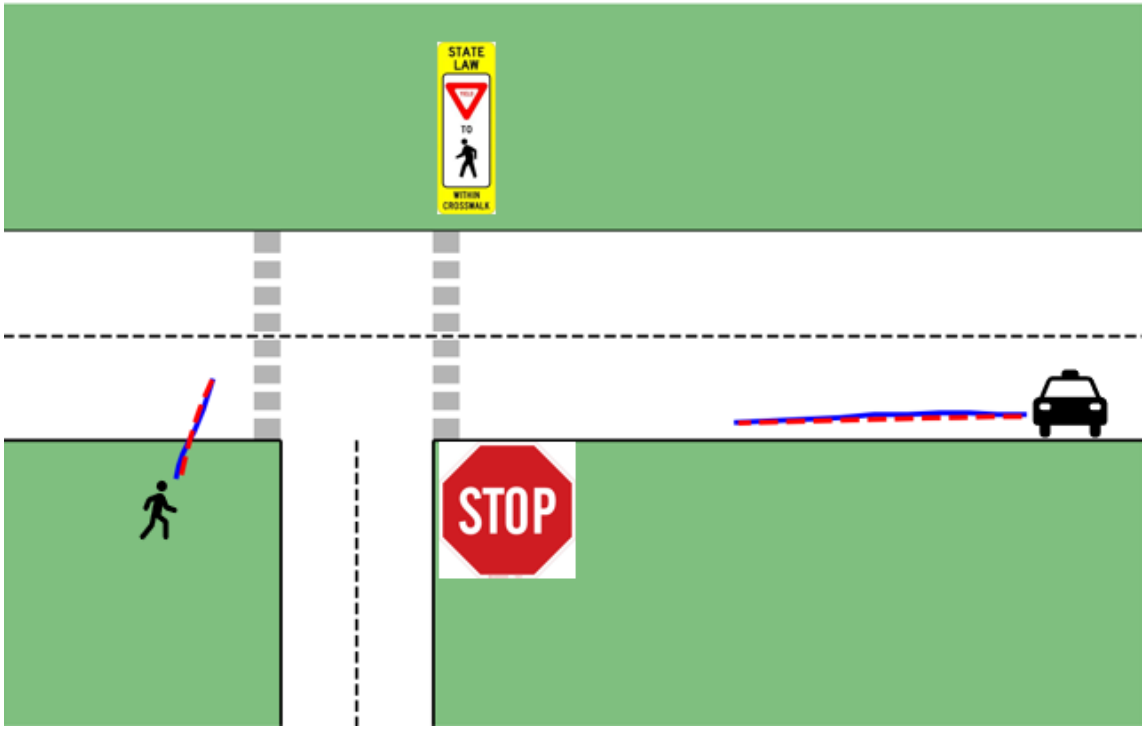

Figure 18 Trajectory Predictions in Pedestrian-Vehicle Interaction Scenario

5.5.2 Hybrid Interactions Scenario 1

For a more complex traffic environment, Figure 19a indicates the ST-GCN-Seq2Seq can reasonably predict road users' future trajectories. Recall that the blue solid lines indicate the ground truth future trajectories (3s) for road users, and the red scatter plots represent the predicted future trajectories (3s) for road users:

Vehicle No. 1 on 2nd Street had to stop and wait for the approaching vehicle on University St. The red dots in Figure 19b demonstrate that the model successfully predicts the "waiting" behavior of the vehicle on 2nd Street.

Pedestrian No. 5 just finishes crossing, and vehicle No. 2 on University Street yields to the subject pedestrian. Pedestrian No. 5 leaves the crosswalk. Vehicle No. 2 accelerates to leave the crossing area. The ST-GCN-Seq2Seq reasonably captures the acceleration behavior of Vehicle No. 2 (the gap between consecutive red points is increasing in Figure 19b) but does not precisely represent the magnitude of the acceleration.

Vehicle No. 3 is following Vehicle No. 2. Due to the yielding behavior of Vehicle No. 2, the ST-GCN-Seq2Seq reasonably predicts the “deceleration” behavior of Vehicle No. 3 (the gap between consecutive red points is increasing) to avoid a rear-end collision. See the red dots for Vehicle No. 3 in Figure 19b.

Vehicle No. 4 is following Vehicle No. 3. The ST-GCN-Seq2Seq accurately predicts that Vehicle No.4 will keep a constant speed, because there is a significant distance between Vehicle No. 3 and Vehicle No. 4. See Figure 19b.

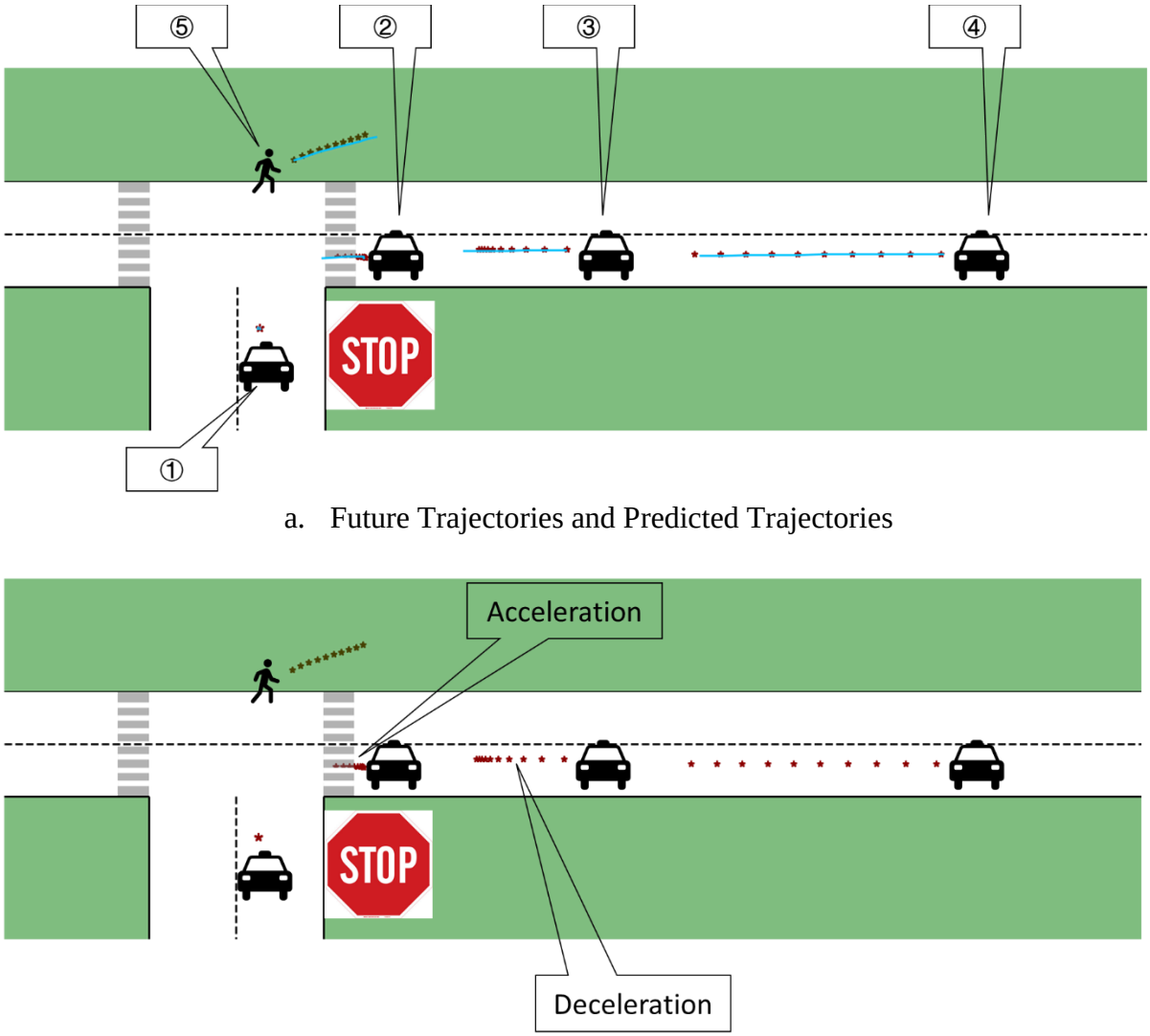

a. Future Trajectories and Predicted Trajectories

b. Predicted Trajectories

Figure 19 Trajectory Predictions in Hybrid Interactions Scenario 1

5.5.3 Hybrid Interactions Scenario 2

Figure 20 indicates that the ST-GCN-Seq2Seq can reasonably predict road users' future trajectories in another complex traffic environment.

Vehicle No. 5 on University Street yields to the subject pedestrians on the crosswalk or in the curb areas. The ST-GCN-Seq2Seq reasonably captures the yielding behavior of Vehicle No. 5 (see red points of Vehicle No. 5 in Figure 20).

The ST-GCN-Seq2Seq precisely predicts the future movements of Pedestrians No. 3 and No. 4 (see red scatter plots of Pedestrians No. 3 and No. 4).

The prediction results for Pedestrian No. 2 are interesting. The Pedestrian No. 2 has conflicts with Pedestrians No. 3 and No. 4. Pedestrian No. 2 actually takes "evasive" behavior to avoid a collision with conflicting pedestrians (see the blue solid line of Pedestrian No. 2 in Figure 20). The ST-GCN-Seq2Seq successfully predicts the "evasive" behavior of Pedestrian No. 2. See the red dots for Pedestrian No. 2 in Figure 20.

However, we should report that the predicted trajectory of Pedestrian No. 1 is reasonable but not accurate. Before stepping into the crosswalk, Pedestrian No. 1 hesitates and "negotiates" with Vehicle No. 5 while in the curb area (see the blue solid line of Pedestrian No. 1 in Figure 20). But the ST-GCN-Seq2Seq directly predicts that Pedestrian No. 1 will step into the crosswalk immediately and accelerate (the gap between consecutive red points is increasing). In this case, complementary information using visual (head, facial expressions, and gaze direction) and map-based cues can be captured in Module 2 to improve the accuracy of predictions.

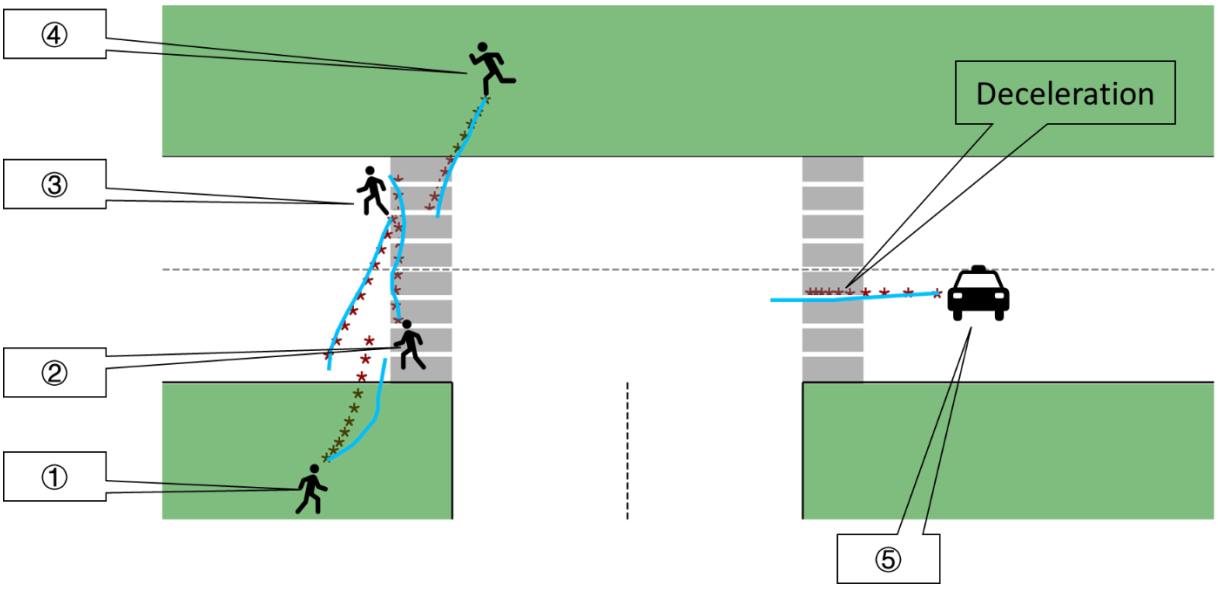

Figure 20 Trajectory Predictions in Hybrid Interactions Scenario 2

5.6 Discussion

A spatial temporal graph convolutional network-based sequence-to-sequence (ST-GCN-Seq2Seq) model has been developed to encode observed road users' movements and predict their future trajectories, considering interactions between heterogeneous road users.

5.6.1 Contributions

This chapter offers a hands-on approach (ST-GCN-Seq2Seq) to predict the movements heterogeneous road users. Experiment results indicate that the proposed ST-GCN-Seq2Seq model outperforms state-of-the-art models in predicting the movements of road users near crosswalks. Three case studies have been conducted to demonstrate the robustness of the proposed ST-GCN-Seq2Seq model that accurately predicts future movements and interactions between heterogeneous road users.

But how do detection and tracking modules, along with motion predictions, help design an intelligent tracking system at smart crosswalks? A three-step strategy suggests itself:

1. The appropriate sensor can be deployed to capture the spatial-temporal coordinates of each road user. In this research, an on-site camera is enough. Emerging technologies such as Miovision (https://miovision.com/) will be more helpful.

2. A computer or smartphone application incorporated with detection and tracking modules along with ST-GCN-Seq2Seq will perform the detection, tracking, and prediction.
3. Pedestrians and cyclists who download the smartphone application can be notified of real-time future trajectory predictions of surrounding road users (pedestrians, cyclists, and motorists). Real-time future trajectory predictions can be utilized as a fine-tuned version of the real-time conflict risk assessment mentioned in Section 4.8.1.

How does ST-GCN-Seq2Seq help achieve a form of "smart interaction" in practice? Trajectory predictions can inform road users of the surrounding environment and other road users' decisions in real time. Several examples are enumerated:

1. In Figure 18, because a low vehicle speed can be inferred from the predicted vehicle trajectory, the pedestrian will cross without hesitation, and the vehicle can keep a constant speed and move across the crosswalk.
2. In Figure 19, if the "deceleration" behavior of Vehicle No. 3 is accurately predicted and the information is sent to Vehicle No. 4, Vehicle No. 4 can prepare to decelerate in advance to avoid an abrupt brake or a full stop.
3. In Figure 20, if the yield behavior of Vehicle No. 5 is accurately predicted and the information is sent to pedestrians, all pedestrians will cross without hesitation or stopping. The predicted yield behavior will help reduce the probabilities of confusion and conflict (Equations 16 and 17) derived from the "zebra-crossing" game.

5.6.2 Future Directions

As more data is collected and fed into the ST-GCN-Seq2Seq framework, the model results are expected to be improved. In addition, complementary information using visual (such as facial expressions and gaze estimations) and map-based cues can be captured in detection and tracking modules to improve the accuracy of motion predictions.

6. OPTIMAL TRAFFIC CONTROL STRATEGY AT CROSSWALKS

This chapter is based on a published conference paper: Zhang, Y., & Fricker, J. (2021, June). Investigating Smart Traffic Signal Controllers at Signalized Crosswalks: A Reinforcement Learning Approach. In 2021 7th International Conference on Models and Technologies for Intelligent Transportation Systems (MT-ITS) (pp. 1-6). IEEE.

At signalized crosswalks, traditional TSCs are easy to implement because they are pretimed or programmed to follow a specific control logic. However, actual traffic conditions are ignored in traditional TSCs, which may result in traffic congestion. This is especially true at crosswalks where pedestrian arrival rates fluctuate widely, such as near universities. During times when classes are beginning and/or ending, pedestrian flow has short-lived but significant peaks. Pretimed control cannot guarantee priority to pedestrians when pedestrian flow is heavy, which causes longer pedestrian delay. Moreover, even though pedestrian-actuated buttons give priority (after some delay) to pedestrians when large numbers of pedestrians are present, they have been observed to seize the priority from drivers, leading to frequently interrupted traffic flow, increased vehicle delay, and safety issues. Therefore, utilizing predefined or pre-programmed TSCs is unlikely to account for temporal variations in real traffic at signalized crosswalks.

To address the limitations of pretimed or pushbutton-actuated TSCs, “smart” pedestrian signals have been proposed. Promising alternatives include reinforcement learning (RL). In the RL framework, a TSC can be considered an agent that interacts with an environment through a sequence of observations, actions, and rewards. The objective of the agent is to choose the optimal sequence of actions that minimizes total delay. A comparison of RL-based TSCs and traditional TSCs will be conducted to demonstrate the relative efficiency of the alternative control strategies.

6.1 Reinforcement Learning Framework

In the reinforcement learning framework, we consider the signal controller as a learning agent. The agent interacts with the simulation environment at each time step t with an observed state of S_t. See Figure 21.

Then the agent chooses an action of A_t that leads to a transition of the environment to the next state of S_{t+1}. After the transition, a reward of r_{t+1} is obtained to quantify the consequence of the action.

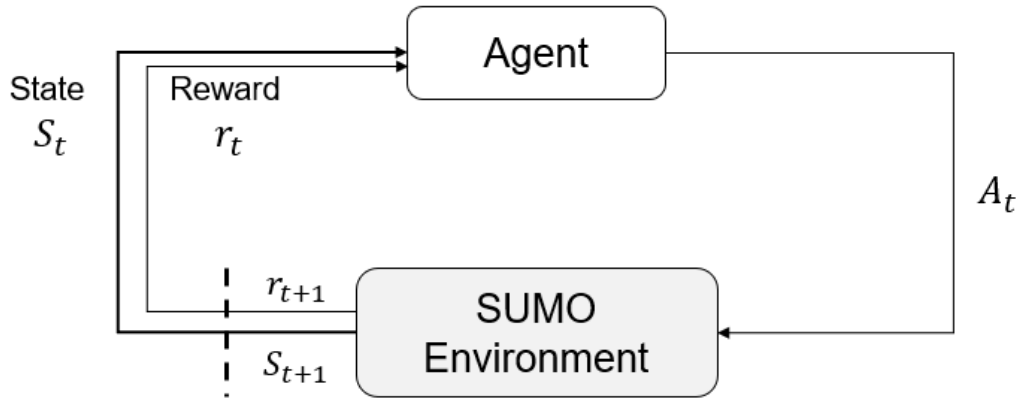

Figure 21 Agent-Environment Framework

The Markov decision process is a mathematical framework that defines the agent-environment structure in Figure 21.

6.2 Markov Decision Process

The Markov decision process can be expressed as $\{S, A, P_a, R_a\}$.

6.2.1 State

The state space $S_t \in (S_{veh,t} \times S_{ped,t})$ consists of two subspaces, $S_{ped,t}$ and $S_{veh,t}$:

1. $S_{ped,t}$ denotes the pedestrian state space that measures the total number of pedestrians waiting in curb areas (with zero velocity) at each time step.

2. $S_{veh,t}$ represents the vehicle state space that measures the total number of vehicles in the queue at each time step. It counts the number of vehicles with zero speed at the intersection.

For example, if the total number of waiting pedestrians ($S_{ped,t}$ = 8), and the number of vehicles in the queue ($S_{veh,t}$ = 5), the state at time step *t* can be represented in Table 8.

Table 8 State Representation

	0	1	2	3	4	5	6	7	8	≥9
$S_{ped,t}$	0	0	0	0	0	0	0	0	1	0
$S_{veh,t}$	0	0	0	0	0	1	0	0	0	0

6.2.2 Action

There are two actions – $\{A_{1,t}, A_{2,t}\}$ representing two green signals.

1. $A_{1,t}$ represents the display of the pedestrian green signal a certain time *t* in the pedestrian walking area. The pedestrian green duration is exactly 25 seconds, with the traffic signal on Northwestern Avenue turning red.
2. Action $A_{2,t}$ displays a vehicle green signal at a certain time *t* on Northwestern Avenue. Vehicle green signal duration is exactly 25 seconds, with the pedestrian signal turning red (Don't Walk).

If the action chosen in time step *t* is the same as the action taken in the last time step *t*-1, the current green phase will persist. On the contrary, if the action chosen in time step *t* is different from the previous action, a three-second yellow phase is triggered, and a two-second all-red interval follows.

6.2.3 Reward

Traffic delay is a critical performance measure in the project-level traffic management. Therefore, the main objective of this study is to investigate a smart traffic control strategy to minimize the total delay at the intersection. We first define the total cumulative wait time (or delay) as:

$$TCWT_t = \sum_i PersonsDelay_{i,t} + \sum_j PedDelay_{j,t} \quad (28)$$

where $PersonsDelay_{i,t}$ denotes the number of persons in vehicles in a queue on the approach i at each time step t. We assumed 1.134 persons per vehicle in this study. The number was chosen based on the average vehicle occupancy rate for home-based work trips from the last vehicle occupancy study in Tippecanoe County, Indiana (2010). Variable $PedDelay_{j,t}$ represents the number of pedestrians waiting in the curb area j at each time step t. There are two curb areas at the intersection: the north curb area and the south curb area. See Figure 8. Then, the proposed reward function can be derived as a function of traffic delay to measure the intersection efficiency in Equation 29.

$$R_t = TCWT_{t-1} - TCWT_t \tag{29}$$

We use the difference in cumulative waiting times between two consecutive time steps (t-1 and t) as the reward function. A negative reward represents a bad action, which means more vehicles are added to the queue or more pedestrians are waiting. A positive reward represents a good action, resulting in less cumulative delay compared to the previous time step.

6.2.4 Learning Mechanism

Q-Learning is an off-policy reinforcement learning algorithm. The task of Q-learning is to find an optimal policy that maximizes the expected total reward (Watkins and Dayan, 1992).

Q-Learning

The Q value calculates the quality of the state-action pair at each time step based on the Bellman optimality equations (Bellman and Dreyfus, 2015). The Bellman equation is defined as:

$$V(s) = max_a\left(R(s,a) + \gamma \sum_{s'} P(s,a,s')\, V(s') \right) \tag{30}$$

where,

1. The value function at state s ($V(s)$) represents how good it is for the agent to be in state s. This is also called optimal cost-to-go at state s.
2. $R(s, a)$ is the immediate reward for taking action a from state s.

3. γ denotes the discount factor.
4. $P(s, a, s')$ represents the transition probability of going from s to s' after executing the action a following the policy π.
5. $V(s')$ is the value function at the next state s'.

By discarding the max function in Equation (30), $Q(s, a)$ is defined to evaluate the quality of each state-action pair:

$$\begin{cases} V(s) = max_a(Q(s,a)) \\ Q(s,a) = R(s,a) + \gamma \sum_{s'} P(s,a,s')\, V(s') \\ Q(s,a) = R(s,a) + \gamma \sum_{s'} P(s,a,s')\, max_{a'}(Q(s',a')) \end{cases} \tag{31}$$

Because both vehicle arrival and pedestrian arrival are stochastic, the reward-to-go the agent gets at time t ($Q_t(s,a)$) may be different from a previous observation at t_{prev} ($Q_{t_{prev}}(s,a)$). Temporal difference learning is introduced as:

$$TD(s,a) = Q_t(s,a) - Q_{t_{prev}}(s,a) \tag{32}$$

The new Q value is updated based on Equation (32):

$$\begin{cases} Q_t(s,a) = Q_{t_{prev}}(s,a) + \alpha TD(s,a) \\ Q_t(s,a) = Q_{t_{prev}}(s,a) + \alpha\left(R(s,a) + \gamma \sum_{s'} P(s,a,s')\, max_{a'} Q(s',a') - Q_{t_{prev}}(s,a)\right) \end{cases} \tag{33}$$

State transition probabilities $P(s, a, s')$ are not usually known in the real world. Instead, state transitions can be simulated in the SUMO software (see Figure 8). Therefore, equation (33) can be generalized as:

$$Q_t(s,a) = Q_{t_{prev}}(s,a) + \alpha\left(R(s,a) + \gamma max_{a'} Q(s',a') - Q_{t_{prev}}(s,a)\right) \tag{34}$$

where a is the learning rate. In this study, a higher discount factor $\gamma = 0.95$ was chosen to highlight the importance of future rewards because we are looking forward to minimizing the total delay over the time period.

Deep Q Network

Q-values are stored and updated in a table. However, an increase in the number of states will increase the amount of memory needed to save and update the Q table. When the number of states is large, it is computationally inefficient to directly update the Q table. To obtain Q-values efficiently, the deep Q-network (DQN) with experience replay has been proposed to approximate the value function $Q(s, a)$ with the vector of parameters θ, using the deep neural network (Mnih et al., 2015). The target value $R(s, a), + \gamma \max_{a'} Q(s', a')$ is replaced by $y = R(s, a), + \gamma \max_{a'} Q(s', a', \theta_i^-)$, where θ_i^- is derived from the previous iteration. $Q(s, a, \theta_i)$ is the predicted Q value at the current iteration. The objective is to minimize the mean squared error (MSE):

$$L_i(\theta_i) = \mathrm{E}_{s,a,r,s'}\left[(y - Q(s,a,\theta_i))^2\right] \tag{35}$$

The input of the DQN is the state of the environment at time t, s_t, and the output of the DQN is the vector of Q-values that take input of possible actions (a_t) at the current state (s_t). The neural network structure is shown in Figure 22. The proposed neural network consists of four fully connected hidden layers with the rectified linear unit (ReLU) as the activation function. Each hidden layer has 400 neurons.

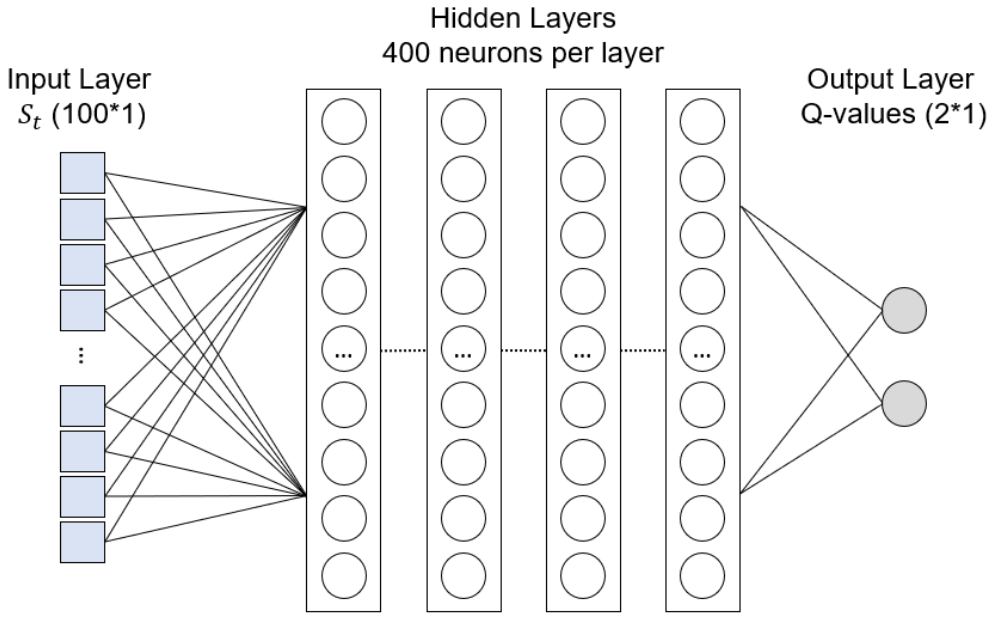

Figure 22 Deep Q Network

Experience Replay

In this study, the agent's experiences, $e_t = (s_t, a_t, r_t, s_{t+1})$, were obtained using traffic simulations. However, the sequence of experiences (e_t) can be highly correlated as traffic simulations are conducted (Mnih et al., 2015). To randomize the training data (experiences) and break down temporal dependencies, a replay buffer is initiated. The replay buffer contains a collection of experiences, $e_t = (s_t, a_t, r_t, s_{t+1})$. The experiences are gradually added to the buffer as traffic simulations are conducted. The Q-learning takes advantage of samples that are pooled uniformly from the dataset ($s, a, r, s' \sim U(D)$) in each iteration.

ε-greedy Policy

In this study, the ε-greedy policy was adopted. Under ε-greedy policy, the agent will choose the action that maximizes the $Q(s, a)$ with the probability of 1-ε. With the probability of ε, the agent will randomly choose an action. ε was chosen as a decreasing function in this study:

$$\varepsilon = 1 - \frac{e}{E} \tag{36}$$

where e is the current training episode and E denotes the total number of episodes. The parameter ε descends uniformly from 1 to 0 during the training process. At the beginning of training, the agent does not know which actions are optimal. Therefore, in the early stages of training, the agent should explore the consequences of its actions. After sufficient explorations, the agent is supposed to exploit what it has learned from previous episodes and choose the optimal action that maximizes the Q value with a high probability.

6.3 Traffic Control Strategies

Three different control strategies were compared in this study.

6.3.1 Fixed-Time Control (Strategy 1)

The fixed-time traffic signal plan at the Northwestern Crosswalk is shown in Table 9. We simulated 1000 experiments with different seeds (seeds 1-1000).

Table 9 Fixed-Time Traffic Signal Plan

Interval Number	Northwestern Ave.		Crosswalk
	N/S Through	N/S Left	E/W Through
1	Green = 25	Red	Red
2	Yellow = 3	Red	Red
3	Red = 2	Red	Red
4	Red	Green = 25	Green = 25
5	Red	Yellow = 3	Yellow = 3
6	Red	Red = 2	Red = 2

6.3.2 Actuated Control Strategy (Strategy 2)

Unlike Strategy 1, waiting pedestrians can actuate a change in signal by pressing or "clicking" a button in the curb area. This strategy follows the traffic signal plan listed in Table 9 except for Interval 1. Interval 1 has a *minimum green time* of 25 seconds in this strategy. If there is at least one pedestrian clicking the button, and Interval 1 has lasted longer than 25 seconds (i.e., green rest status), the signal will switch to the next interval immediately. Also, 1000 experiments with different seeds (seeds 1-1000) were generated in the SUMO simulation.

6.3.3 Smart Control Strategy (Strategy 3)

The proposed reinforcement learning framework is called a "smart control strategy". Table 10 lists the parameters used in the reinforcement learning framework. The smart traffic signal plan has two separate phases. Phase 1 is grouped with Intervals 1, 2, and 3 in Table 9. Phase 2 is clustered with Intervals 4, 5, and 6 in Table 9. Each phase is an action defined in Section 6.2.2. 1000 episodes (seeds 1-1000) are simulated in the SUMO environment.

Table 10 Training Settings

Parameters	Value
Simulation	
Total Episodes	1000
Maximum Time Steps	3600 seconds
Green Duration	25 seconds
Yellow Duration	3 seconds
All-Red Interval	2 seconds
Model	

Number of Layers	4
Neurons per Layer	400
Batch Size	100
Learning Rate	0.001
Training Epochs	1000
Memory	
Minimum	600
Maximum	50000
Agent	
Number of States	100
Number of Actions	2
Discount Factor	0.95

6.4 Experiments and Results

6.4.1 Experiments

Two different model settings are defined and tested:

1. Setting 1: Vehicle arrivals are assumed to follow a Poisson distribution with $\lambda = 0.08$/s, and pedestrian arrivals follow a Binomial distribution $B(5, 1/6)$. In this setting, pedestrian volume is moderate and vehicle volume is low.
2. Setting 2: Vehicle arrivals are assumed to follow a Poisson distribution with $\lambda = 0.35$/s, and pedestrian arrivals follow a Binomial distribution $B(5, 1/6)$. In this setting, pedestrian volume is moderate and vehicle volume is moderate.

Setting 1 was chosen based on the empirical data collection described in Section 3.3. The only difference between Setting 1 and Setting 2 is the vehicle volume. We increase the vehicle arrival rate from $\lambda = 0.08$/s to 0.35/s in order to attest a different combination of pedestrian flow rate and vehicle volume in the simulation framework. Three different control strategies (fixed-time control, actuated control, and smart control) have been simulated in each setting.

6.4.2 Results

Supplementary materials such as codes, datasets and plots can be found in the repository from the GitHub link: https://github.com/YZhang-Genghis/deep-reinforcement-learning-pedestrian-signal-design.

Setting 1

We first analyze the results with the moderate pedestrian arrival rate and the low vehicle arrival rate. In Figure 23, the total cumulative waiting time (TCWT) begins at about 11,000 for Strategy 1 (fixed-time control) and at about 7,000 for pedestrian-actuated Strategy 2. This makes sense. Detector-based TSCs allow the vehicle phase to be green if there are no pedestrians waiting to cross. However, as simulation episodes increase, the total delay for Strategies 1 and 2 does not change significantly. This is because traffic signal controllers are following pre-defined plans while no "learning" is taking place. The performance of Smart Control Strategy 3 begins with a TCWT of about 25,000. This inferior value is because Strategies 1 and 2 benefit from having been set by traffic engineers, while "learning" for Strategy 3 has just begun. In early simulation episodes, the exploration rates ε (from Equation 36) are high, and the agent has yet to fully explore the state-action space and consequences of actions. As the training process continues, exploration rates ε linearly decrease. The agent will be greedier to exploit the "optimal" policy learned from previous episodes via the proposed deep Q network. Therefore, the total delay for Strategy 3 gradually decreases, converging to Strategy 1 (fixed-time control) at about 11,000 for the last 100 training episodes. This result confirms the ability of the Smart Control strategy to replicate an existing signal timing plan. It also offers the possibility of producing superior timings as vehicle and pedestrian arrival rates vary.

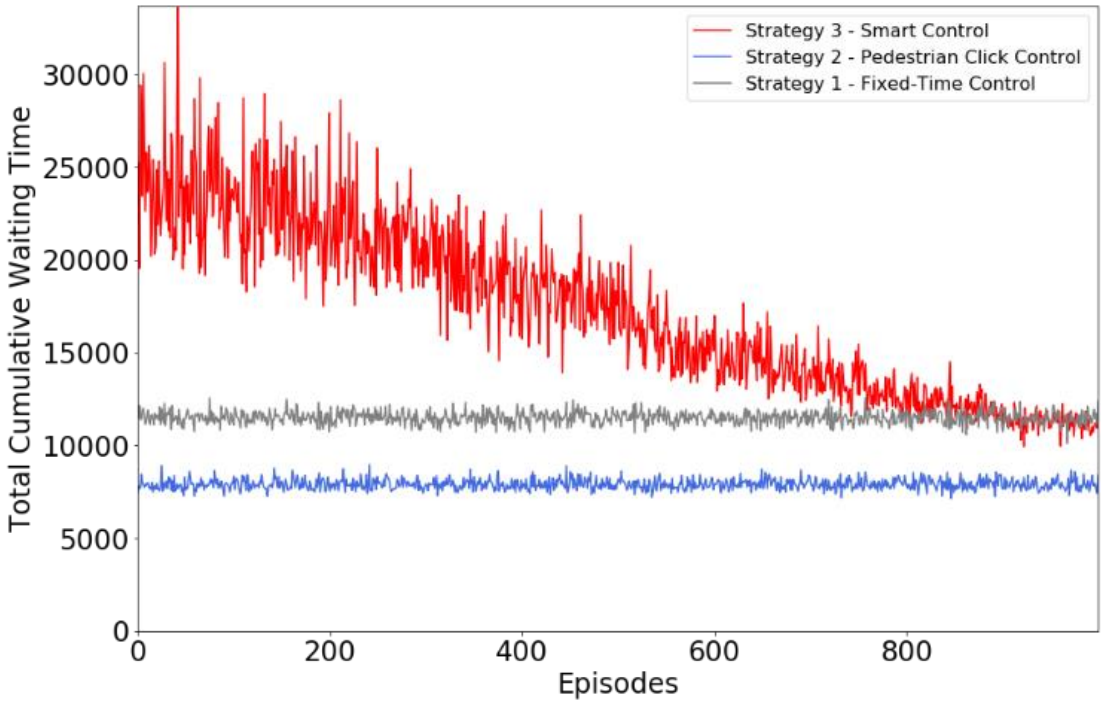

Figure 23 Total Cumulative Waiting Time in Setting 1

Setting 2

We then analyze the results over a period with a moderate pedestrian arrival rate and a moderate vehicle arrival rate. As in Figure 24 for Setting 2, Strategy 3 starts with the highest TCWT (more than 60,000) but eventually outperforms baseline control Strategies 1 and 2, with a TCWT of less than 40,000.

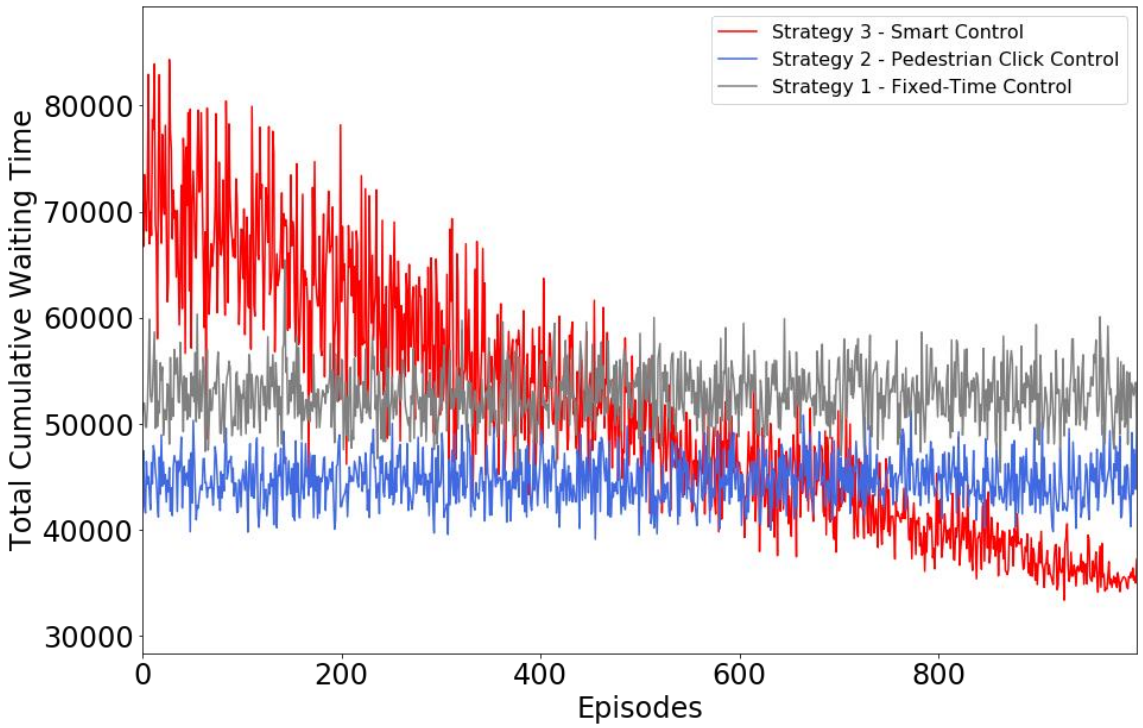

Figure 24 Total Cumulative Waiting Time in Setting 2

6.5 Discussion

6.5.1 Contributions

This study applies an RL framework to find the optimal signal control strategy for a signalized crosswalk in a micro-simulation environment. A DQN with experience replay is

developed to approximate the Q-value. Our analysis after applying the Smart Control Strategy indicates that:

1. As training processes, DQN converges, and the total delay decreases. See Figure 23 and Figure 24.
2. The existing control strategy (Strategy 2) works better in a period with moderate pedestrian volume and low vehicle volume.

The proposed RL framework works well in a period with moderate pedestrian arrival rates and moderate vehicle arrival rates. As an optimized Puffin control shown in

3. , the smart control strategy offers extended vehicle green times without frequently switching from vehicle green signal to pedestrian green signal when pedestrian arrival rates are moderate.
4. The trained deep-Q network in Figure 22 can be converted into a traffic signal flowchart that is practical for TSCs at crosswalks with a moderate pedestrian flow rate and moderate vehicle volume.

The study described in this paper identified the efficiency of several traffic signal control strategies at signalized crosswalks. These findings provide insights into which efficient TSCs are practical. And reinforcement learning traffic signal controllers can be applied at signalized crosswalks to reduce total delay when both vehicle volume and pedestrian flow rate are moderate.

6.5.2 Future Directions

This study presents comparisons of three different signal control strategies in two different combinations of pedestrian flow rate and vehicle volume. In the future, various scheduling settings considering various combinations of pedestrian flow rate and vehicle flow rate can be tested. Moreover, this paper proposes a single-agent, single-objective reinforcement learning framework in terms of efficiency. Safety is also an important performance measure at signalized crosswalks. The RL framework can be extended into a multi-agent, multi-objective reinforcement learning framework.

7. CONCLUSIONS

As documented by hours of video, the assertion of priority results from a silent "social rule" between pedestrian and driver. The video was recorded at three busy "semi-controlled" crosswalks on a university campus.

As the behavior between pedestrians and drivers at a semi-controlled crosswalk is becoming better predicted, how can this information help achieve a form of "smart interaction" at "smart" crosswalks? Our solution was to develop the observing-tracking-learning framework shown in Figure 3:

1. Examples of how to take advantage of sensors (on-site cameras) and how to process the information from sensors have been revealed in Chapter 3. Using computer vision algorithms, the observing and tracking modules generate a large-scale spatial-temporal trajectory dataset that can be commonly used in planning, prediction, and simulation tasks.
2. In Chapter 4, a game-theoretical approach offers a valuable complement to (i) account for the joint behavior of pedestrian and motorist as they negotiate the right-of-way and (ii) infer the effect of explanatory variables on the probability of conflict. A real-time safety assessment framework at semi-controlled crosswalks has been developed.
3. Chapter 5 explores an ST-GCN-Seq2Seq model that encodes observed road users' trajectories and predicts future trajectories in real time. Numerical examples indicate that real-time trajectory predictions can (i) inform road users of surrounding road users' decisions to avoid confusions or conflicts and (ii) achieve a form of smart interaction between heterogeneous road users.

As an extension of the previous studies, pedestrian-motorist intersections with stop signs or signals (controlled crosswalks) have been addressed in Chapter 6. The study was aimed at identifying the efficiency of several traffic signal control strategies at signalized crosswalks. Using reinforcement learning, a "smart" traffic signal controller has been proposed and compared with baseline traffic signal controllers on the basis of traffic efficiency. The "smart" traffic signal

controller can be applied at signalized intersections to reduce total delay when both vehicle volume and pedestrian flow rate are moderate.

Together, the three learning algorithms can provide valuable guidance on the interaction of pedestrians and vehicles at both semi-controlled and controlled crosswalks.

REFERENCES

AASHTO. (2010). Highway safety manual, Washington, DC.

Alahi, A., Goel, K., Ramanathan, V., Robicquet, A., Fei-Fei, L., & Savarese, S. (2016). Social lstm: Human trajectory prediction in crowded spaces. In Proceedings of the IEEE conference on computer vision and pattern recognition (pp. 961-971).

Alsaleh, R., & Sayed, T. (2020). Modeling pedestrian-cyclist interactions in shared space using inverse reinforcement learning. Transportation Research part F: traffic psychology and behaviour, 70, 37-57.

Alver, Y., & Onelcin, P. (2018). Gap acceptance of pedestrians at overpass locations. Transportation Research Part F: Traffic Psychology and Behaviour, 56, 436-443.

Amado, H., Ferreira, S., Tavares, J. P., Ribeiro, P., & Freitas, E. (2020). Pedestrian–Vehicle Interaction at Unsignalized Crosswalks: A Systematic Review. Sustainability, 12(7), 2805.

Arhin S. and Noel E. C. (2010). Evaluation of HAWK Signal at Georgia Avenue and Hemlock Street, NW, in the District of Columbia, District Department of Transportation Planning Policy, Planning and Sustainability Administration, Washington, DC, USA.

Arbis, D., & Dixit, V. V. (2019). Game theoretic model for lane changing: Incorporating conflict risks. Accident Analysis & Prevention, 125, 158-164.

Asaithambi, G., Kuttan, M. O., & Chandra, S. (2016). Pedestrian road crossing behavior under mixed traffic conditions: A comparative study of an intersection before and after implementing control measures. Transportation in Developing Economies, 2(2), 14.

Aslani, M., Seipel, S., Mesgari, M. S., & Wiering, M. (2018). Traffic signal optimization through discrete and continuous reinforcement learning with robustness analysis in downtown Tehran. Advanced Engineering Informatics, 38, 639-655.

Bellman, R. E., & Dreyfus, S. E. (2015). Applied dynamic programming. Princeton university press.

Bhattacharyya, R. P., Phillips, D. J., Wulfe, B., Morton, J., Kuefler, A., & Kochenderfer, M. J. (2018, October). Multi-agent imitation learning for driving simulation. In 2018 IEEE/RSJ International Conference on Intelligent Robots and Systems (IROS) (pp. 1534-1539). IEEE.

Bjørnskau, T. (2017). The Zebra Crossing Game–Using game theory to explain a discrepancy between road user behaviour and traffic rules. *Safety Science*, 92, 298-301.

Blue, V. J., & Adler, J. L. (2001). Cellular automata microsimulation for modeling bi-directional pedestrian walkways. Transportation Research Part B: Methodological, 35(3), 293-312.

Boillot, F., Midenet, S., & Pierrelee, J. C. (2006). The real-time urban traffic control system CRONOS: Algorithm and experiments. Transportation Research Part C: Emerging Technologies, 14(1), 18-38.

Brouwer, L. E. J. (1911). Über abbildung von mannigfaltigkeiten Mathematische Annalen, 71(1), 97-115. (In German, translated in *Wikipedia: The Free Encyclopedia*, s.v. "Brouwer fixed-point theorem").

Camara, F., Bellotto, N., Cosar, S., Weber, F., Nathanael, D., Althoff, M., Wu, J., Ruenz, J., Dietrich, A., Markkula, G., Schieben, A., Tango, F., Merat, N., & Fox, C. (2020). Pedestrian models for autonomous driving part ii: high-level models of human behavior. IEEE Transactions on Intelligent Transportation Systems, 22(9), 5453-5472.

Chang, M. F., Lambert, J., Sangkloy, P., Singh, J., Bak, S., Hartnett, A., Wang, D., Carr., P., Lucey, S., Ramanan, D., & Hays, J. (2019). Argoverse: 3d tracking and forecasting with rich maps. In Proceedings of the IEEE/CVF Conference on Computer Vision and Pattern Recognition (pp. 8748-8757).

Chen, Q., & Wang, Y. (2015). Cellular automata (CA) simulation of the interaction of vehicle flows and pedestrian crossings on urban low-grade uncontrolled roads. *Physica A: Statistical Mechanics and its Applications*, 432, 43-57.

Cheng, Boyu (2015). Study of Pedestrian and Driver Behavior along Northwestern Avenue Before and After Signalization of Crosswalks, CE497 research report, School of Civil Engineering, Purdue University, June 2015. Available from Dr. Jon Fricker.

Cloutier, M. S., Lachapelle, U., d'Amours-Ouellet, A. A., Bergeron, J., Lord, S., & Torres, J. (2017). "Outta my way!" Individual and environmental correlates of interactions between pedestrians and vehicles during street crossings. *Accident Analysis & Prevention*, 104, 36-45.

Cools, S. B., Gershenson, C., & D'Hooghe, B. (2013). Self-organizing traffic lights: A realistic simulation. In Advances in Applied Self-Organizing Systems (pp. 45-55). Springer, London.

Deo, N., & Trivedi, M. M. (2018). Convolutional social pooling for vehicle trajectory prediction. In Proceedings of the IEEE Conference on Computer Vision and Pattern Recognition Workshops (pp. 1468-1476).

Dixit, V. V., & Denant-Boemont, L. (2014). Is equilibrium in transport pure Nash, mixed or Stochastic?. *Transportation Research Part C: Emerging Technologies*, 48, 301-310.

Dutta, U., Bodke, S., Dara, B., and Lynch, J. (2010). "Safety evaluation of SCATS control system." Rep. No. MIOH UTC TS22p1-2 2010-Final, Michigan-Ohio Univ. Transportation Center, Michigan Dept. of Transportation, Lansing, MI.

Ellis, D., Sommerlade, E., & Reid, I. (2009). Modelling pedestrian trajectory patterns with gaussian processes. In 2009 IEEE 12th International Conference on Computer Vision Workshops, ICCV Workshops (pp. 1229-1234). IEEE.

Elnagar, A. (2001). Prediction of moving objects in dynamic environments using Kalman filters. In Proceedings 2001 IEEE International Symposium on Computational Intelligence in Robotics and Automation (Cat. No. 01EX515) (pp. 414-419). IEEE.

Elvik, R. (2014). A review of game-theoretic models of road user behaviour. *Accident Analysis & Prevention*, 62, 388-396.

Fayyaz, K., Schultz, G. G., & Galvez de Leon, P. (2019). Driver Compliance at Enhanced Pedestrian Crossings in Utah (No. UT-19.03). Utah. Dept. of Transportation.

FHWA (Federal Highway Administration). 2014. "Pedestrian hybrid beacon guide—Recommendations and case study." Accessed February 11, 2022. https://safety.fhwa.dot.gov/ped_bike/tools_solve/fhwasa14014/.

Fink, J., Kwigizile, V., & Oh, J. S. (2016). Quantifying the impact of adaptive traffic control systems on crash frequency and severity: Evidence from Oakland County, Michigan. Journal of safety research, 57, 1-7.

Fricker, J. D., & Zhang, Y. (2019). Modeling pedestrian and motorist interaction at semi-controlled crosswalks: the effects of a change from one-way to two-way street operation. Transportation research record, 2673(11), 433-446.

Fu, T., Miranda-Moreno, L., & Saunier, N. (2018). A novel framework to evaluate pedestrian safety at non-signalized locations. Accident Analysis & Prevention, 111, 23-33.

Fujii, H., Uchida, H., & Yoshimura, S. (2017). Agent-based simulation framework for mixed traffic of cars, pedestrians and trams. Transportation research part C: emerging technologies, 85, 234-248.

Garcia-Nieto, J., Olivera, A. C., & Alba, E. (2013). Optimal cycle program of traffic lights with particle swarm optimization. IEEE Transactions on Evolutionary Computation, 17(6), 823-839.

Gartner, N. H. (1983). OPAC: A demand-responsive strategy for traffic signal control (No. 906).

Genders, W., & Razavi, S. (2019). An open-source framework for adaptive traffic signal control. arXiv preprint arXiv:1909.00395.

Gettman, D., & Head, L. (2003). Surrogate safety measures from traffic simulation models. Transportation Research Record, 1840(1), 104-115.

Gettman, D., Pu, L., Sayed, T., & Shelby, S. G. (2008). Documentation of surrogate safety measures from traffic simulation models (FHWA-RD-03050). U.S. Department of Transportation, FHWA

Gipps, P. G., & Marksjö, B. (1985). A micro-simulation model for pedestrian flows. Mathematics and computers in simulation, 27(2-3), 95-105.

Godavarthy, R. P., & Russell, E. R. (2016). Study of pedestrian hybrid beacon's effectiveness for motorists at midblock pedestrian crossings. Journal of Traffic and Transportation Engineering (English Edition), 3(6), 531-539.

González, D., Pérez, J., Milanés, V., & Nashashibi, F. (2015). A review of motion planning techniques for automated vehicles. IEEE Transactions on Intelligent Transportation Systems, 17(4), 1135-1145.

Geiger, A., Lenz, P., Stiller, C., & Urtasun, R. (2013). Vision meets robotics: The kitti dataset. *The International Journal of Robotics Research*, *32*(11), 1231-1237.

Gregoire, J., Qian, X., Frazzoli, E., De La Fortelle, A., & Wongpiromsarn, T. (2014). Capacity-aware backpressure traffic signal control. IEEE Transactions on Control of Network.

Gupta, A., Johnson, J., Fei-Fei, L., Savarese, S., & Alahi, A. (2018). Social gan: Socially acceptable trajectories with generative adversarial networks. In Proceedings of the IEEE Conference on Computer Vision and Pattern Recognition (pp. 2255-2264).

Hassan, S. A., Hounsell, N. B., & Shrestha, B. P. (2013). Verification of puffin modelling using VISSIM. Jurnal Teknologi, 65(3).

He, Q., Head, K. L., & Ding, J. (2014). Multi-modal traffic signal control with priority, signal actuation and coordination. Transportation Research Part C: emerging technologies, 46, 65-82.

Helbing, D., & Molnar, P. (1995). Social force model for pedestrian dynamics. Physical review E, 51(5), 4282.

Heylighen, F., & Gershenson, C. (2003). The meaning of selforganization in computing. IEEE Intelligent Systems, 18(4).

Ho, J., Gupta, J., & Ermon, S. (2016, June). Model-free imitation learning with policy optimization. In International Conference on Machine Learning (pp. 2760-2769). PMLR.

Hunt, P. B., Robertson, D. I., Bretherton, R. D., & Winton, R. I. (1981). SCOOT-a traffic responsive method of coordinating signals (No. LR 1014 Monograph). Systems, 2(2), 164-173.

Ioffe, S., & Szegedy, C. (2015, June). Batch normalization: Accelerating deep network training by reducing internal covariate shift. In International conference on machine learning (pp. 448-456). PMLR.

Joseph, J., Doshi-Velez, F., Huang, A. S., & Roy, N. (2011). A Bayesian nonparametric approach to modeling motion patterns. Autonomous Robots, 31(4), 383-400.

Khattak, Z. H., Fontaine, M. D., Smith, B. L., & Ma, J. (2019). Crash severity effects of adaptive signal control technology: An empirical assessment with insights from Pennsylvania and Virginia. Accident Analysis & Prevention, 124, 151-162.

Khattak, Z. H., Magalotti, M. J., & Fontaine, M. D. (2018). Estimating safety effects of adaptive signal control technology using the Empirical Bayes method. Journal of safety research, 64, 121-128.

Kingma, D. P., & Ba, J. (2014). Adam: A method for stochastic optimization. arXiv preprint arXiv:1412.6980.

Kim, B., Kang, C. M., Kim, J., Lee, S. H., Chung, C. C., & Choi, J. W. (2017). Probabilistic vehicle trajectory prediction over occupancy grid map via recurrent neural network. In 2017 IEEE 20th International Conference on Intelligent Transportation Systems (ITSC) (pp. 399-404). IEEE.

Kipf, T. N., & Welling, M. (2016). Semi-supervised classification with graph convolutional networks. arXiv preprint arXiv:1609.02907.

Kuefler, A., Morton, J., Wheeler, T., & Kochenderfer, M. (2017, June). Imitating driver behavior with generative adversarial networks. In 2017 IEEE Intelligent Vehicles Symposium (IV) (pp. 204-211). IEEE.

LeCun, Y., & Bengio, Y. (1995). Convolutional networks for images, speech, and time series. The handbook of brain theory and neural networks, 3361(10), 1995.

Lee, J., Abdulhai, B., Shalaby, A., & Chung, E. H. (2005). Real-time optimization for adaptive traffic signal control using genetic algorithms. Journal of Intelligent Transportation Systems, 9(3), 111-122.

Li, Y., Song, J., & Ermon, S. (2017, December). InfoGAIL: interpretable imitation learning from visual demonstrations. In Proceedings of the 31st International Conference on Neural Information Processing Systems (pp. 3815-3825).

Li, X., Ying, X., & Chuah, M. C. (2019). Grip: Graph-based interaction-aware trajectory prediction. In 2019 IEEE Intelligent Transportation Systems Conference (ITSC) (pp. 3960-3966). IEEE.

Lopez, P. A., Behrisch, M., Bieker-Walz, L., Erdmann, J., Flötteröd, Y. P., Hilbrich, R., Lücken, L., Rummel, J., Wagner, P., & Wießner, E. (2018, November). Microscopic traffic simulation using sumo. In 2018 21st International Conference on Intelligent Transportation Systems (ITSC) (pp. 2575-2582). IEEE

Lowrie, P. R. (1990). Scats, Sydney coordinated adaptive traffic system: A traffic responsive method of controlling urban traffic.

Lu, L., Ren, G., Wang, W., Chan, C. Y., & Wang, J. (2016). A cellular automaton simulation model for pedestrian and vehicle interaction behaviors at unsignalized mid-block crosswalks. Accident Analysis & Prevention, 95, 425-437.

Luyanda, F., Gettman, D., Head, L., Shelby, S., Bullock, D., & Mirchandani, P. (2003). ACS-Lite algorithmic architecture: applying adaptive control system technology to closed-loop traffic signal control systems. Transportation Research Record, 1856(1), 175-184.

Ma, J., Fontaine, M. D., Zhou, F., Hu, J., Hale, D. K., & Clements, M. O. (2016). Estimation of crash modification factors for an adaptive traffic-signal control system. Journal of transportation engineering, 142(12), 04016061.

Ma, Y., Zhu, X., Zhang, S., Yang, R., Wang, W., & Manocha, D. (2019, July). Trafficpredict: Trajectory prediction for heterogeneous traffic-agents. In Proceedings of the AAAI Conference on Artificial Intelligence (Vol. 33, No. 01, pp. 6120-6127).

Mannering, F. L., Shankar, V., & Bhat, C. R. (2016). Unobserved heterogeneity and the statistical analysis of highway accident data. Analytic methods in accident research, 11, 1-16.

Mannion, P., Duggan, J., & Howley, E. (2016). An Experimental Review of Reinforcement Learning Algorithms for Adaptive Traffic Signal Control. Autonomic Road Transport Support Systems, 47.

Marisamynathan, S., & Vedagiri, P. (2018). Modeling pedestrian crossing behavior and safety at signalized intersections. Transportation research record, 2672(31), 76-86.

McKelvey, R. D., & Palfrey, T. R. (1995). Quantal response equilibria for normal form games. *Games and Economic Behavior*, *10*(1), 6-38.

Mikami, S., & Kakazu, Y. (1994, June). Genetic reinforcement learning for cooperative traffic signal control. In Proceedings of the First IEEE Conference on Evolutionary Computation. IEEE World Congress on Computational Intelligence (pp. 223-228). IEEE.

Millard-Ball, A. (2018). Pedestrians, autonomous vehicles, and cities. Journal of Planning Education and Research, 38(1), 6-12.

Mirchandani, P., & Head, L. (2001). A real-time traffic signal control system: architecture, algorithms, and analysis. Transportation Research Part C: Emerging Technologies, 9(6), 415-432.

Mnih, V., Kavukcuoglu, K., Silver, D., Rusu, A. A., Veness, J., Bellemare, M. G., et al. (2015). Human-level control through deep reinforcement learning. nature, 518(7540), 529-533.

Mousavi, S. S., Schukat, M., & Howley, E. (2017). Traffic light control using deep policy-gradient and value-function-based reinforcement learning. IET Intelligent Transport Systems, 11(7), 417-423.

Nascimento, J. C., Figueiredo, M. A., & Marques, J. S. (2009). Trajectory classification using switched dynamical hidden Markov models. IEEE Transactions on Image Processing, 19(5), 1338-1348.

Pawar, D. S., Patil, G. R., Chandrasekharan, A., & Upadhyaya, S. (2015). Classification of gaps at uncontrolled intersections and midblock crossings using support vector machines. *Transportation Research Record*, 2515(1), 26-33.

Pawar, D. S., & Patil, G. R. (2016). Critical gap estimation for pedestrians at uncontrolled mid-block crossings on high-speed arterials. *Safety Science*, 86, 295-303.

Previtali, F., Bordallo, A., Iocchi, L., & Ramamoorthy, S. (2016, December). Predicting future agent motions for dynamic environments. In 2016 15th IEEE International Conference on Machine Learning and Applications (ICMLA) (pp. 94-99). IEEE.

PTV Group, (2021). Areas of Application for PTV Vissim. Available from: https://www.ptvgroup.com/en/solutions/products/ptv-vissim/areas-of-application/. Access date: 2021-12-18.

Rasouli, A., & Tsotsos, J. K. (2019). Autonomous vehicles that interact with pedestrians: A survey of theory and practice. IEEE transactions on intelligent transportation systems, 21(3), 900-918.

Ricalde, E., & Banzhaf, W. (2017). Evolving adaptive traffic signal controllers for a real Strategy using genetic programming with an epigenetic mechanism. In 2017 16th IEEE International Conference on Machine Learning and Applications (ICMLA) (pp. 897-902). IEEE.

Rudenko, A., Palmieri, L., Herman, M., Kitani, K. M., Gavrila, D. M., & Arras, K. O. (2020). Human motion trajectory prediction: A survey. The International Journal of Robotics Research, 39(8), 895-935.

Sacchi, E., Sayed, T., & El-Basyouny, K. (2016). A full Bayes before-after study accounting for temporal and spatial effects: Evaluating the safety impact of new signal installations. Accident Analysis & Prevention, 94, 52-58.

Schroeder, B. J., & Rouphail, N. M. (2010). Event-based modeling of driver yielding behavior at unsignalized crosswalks. *Journal of Transportation Engineering*, 137(7), 455-465.

Schroeder, B. J., & Rouphail, N. M. (2011). Empirical behavioral models to support alternative tools for the analysis of mixed-priority pedestrian-vehicle interaction in a highway capacity context. *Procedia-Social and Behavioral Sciences*, 16, 653-663.

Stevanovic, A., Stevanovic, J., & Kergaye, C. (2013). Optimization of traffic signal timings based on surrogate measures of safety. Transportation research part C: emerging technologies, 32, 159-178.

Stevanovic, A., Stevanovic, J., So, J., & Ostojic, M. (2015). Multi-criteria optimization of traffic signals: Mobility, safety, and environment. Transportation Research Part C: Emerging Technologies, 55, 46-68.

Sucha, M., Dostal, D., & Risser, R. (2017). Pedestrian-driver communication and decision strategies at marked crossings. Accident Analysis & Prevention, 102, 41-50.

Talebpour, A., Mahmassani, H. S., & Hamdar, S. H. (2015). Modeling lane-changing behavior in a connected environment: A game theory approach. *Transportation Research Part C: Emerging Technologies*, 59, 216-232.

Tarko, A. P. (2021). A unifying view on traffic conflicts and their connection with crashes. Accident Analysis & Prevention, 158, 106187.

Torabi, F., Warnell, G., & Stone, P. (2018, July). Behavioral cloning from observation. In Proceedings of the 27th International Joint Conference on Artificial Intelligence (pp. 4950-4957).

Train, K. E. (2009). Discrete choice methods with simulation. Cambridge university press.

Varaiya, P. (2013). The max-pressure controller for arbitrary networks of signalized intersections. In Advances in Dynamic Network Modeling in Complex Transportation Systems (pp. 27-66). Springer, New York, NY.

Vemula, A., Muelling, K., & Oh, J. (2018, May). Social attention: Modeling attention in human crowds. In 2018 IEEE international Conference on Robotics and Automation (ICRA) (pp. 4601-4607). IEEE.

Watling, D. (2006). User equilibrium traffic network assignment with stochastic travel times and late arrival penalty. *European Journal of Operational Research*, 175(3), 1539-1556.

Watkins, C. J., & Dayan, P. (1992). Q-learning. Machine learning, 8(3-4), 279-292.

Webster, F. V. (1958). Traffic signal settings (No. 39).

Wongpiromsarn, T., Uthaicharoenpong, T., Wang, Y., Frazzoli, E., & Wang, D. (2012, September). Distributed traffic signal control for maximum network throughput. In 2012 15th international IEEE Conference on Intelligent Transportation Systems (pp. 588-595). IEEE

Wu, C. J. (1983). On the convergence properties of the EM algorithm. *The Annals of Statistics*, 95-103.

Wu, F., Chen, H., Hou, K., Cheng, Z., & Qiu, T. Z. (2022). Adaptive Pushbutton Control for Signalized Pedestrian Midblock Crossings. Journal of Transportation Engineering, Part A: Systems, 148(4), 04022011.

Yan, S., Xiong, Y., & Lin, D. (2018, April). Spatial temporal graph convolutional networks for skeleton-based action recognition. In Thirty-second AAAI conference on artificial intelligence.

Yu, F., Chen, H., Wang, X., Xian, W., Chen, Y., Liu, F., ... & Darrell, T. (2020). Bdd100k: A diverse driving dataset for heterogeneous multitask learning. In Proceedings of the IEEE/CVF conference on computer vision and pattern recognition (pp. 2636-2645).

Zeng, W., Chen, P., Nakamura, H., & Iryo-Asano, M. (2014). Application of social force model to pedestrian behavior analysis at signalized crosswalk. Transportation research part C: emerging technologies, 40, 143-159.

Zhang, Y. (2019). Pedestrian-Vehicle Interactions at Semi-Controlled Crosswalks: Explanatory Metrics and Models (Master's Thesis, Purdue University Graduate School).

Zhang, C., Chen, F., & Wei, Y. (2019). Evaluation of pedestrian crossing behavior and safety at uncontrolled mid-block crosswalks with different numbers of lanes in China. *Accident Analysis & Prevention*, 123, 263-273.

Zhang, Y., Qiao, Y., & Fricker, J. D. (2020). Investigating Pedestrian Waiting Time at Semi-Controlled Crossing Locations: Application of Multi-State Models for Recurrent Events Analysis. Accident Analysis & Prevention, 137, 105437.

Zhang, Y., & Fricker, J. D. (2020). Multi-State Semi-Markov Modeling of Recurrent Events: Estimating Driver Waiting Time at Semi-Controlled Crosswalks. Analytic Methods in Accident Research, 100131.

Zhang, Y., & Fricker, J. D (2021). Investigating temporal variations in pedestrian crossing behavior at semi-controlled crosswalks: A Bayesian multilevel modeling approach. Transportation Research Part F: Traffic Psychology and Behaviour, 76, 92-108.

Zhang, Y., & Fricker, J. D. (2021). Incorporating conflict risks in pedestrian-motorist interactions: A game theoretical approach. Accident Analysis & Prevention, 159, 106254.

Ziebart, B. D., Ratliff, N., Gallagher, G., Mertz, C., Peterson, K., Bagnell, J. A., Hebert, M., Dey, A. K., & Srinivasa, S. (2009, October). Planning-based prediction for pedestrians. In 2009 IEEE/RSJ International Conference on Intelligent Robots and Systems (pp. 3931-3936). IEEE.

Zhi, W., Ott, L., & Ramos, F. (2020). Kernel trajectory maps for multi-modal probabilistic motion prediction. In Conference on Robot Learning (pp. 1405-1414). PMLR.

APPENDIX

Table 11 Estimation Results for Model Parameters with Additional Data

Parameter and Variable	Coefficient	Bootstrap Standard Deviation	z_score	$P > \|z\|$
a_1 V_{ped}^2	0.094782	0.014705	6.445568	1.15E-10
a_2	0.936	0.432958	2.16187	0.030628
a_3 d_{ped}	-0.03363	0.0087	-3.86588	0.000111
a_4 d_{ped}^2	0.00016	3.63E-05	4.396481	1.10E-05
a_5 d_{veh}	0.080244	0.013082	6.134145	8.56E-10
a_6 d_{veh}^2	-0.0003	5.84E-05	-5.17881	2.23E-07
a_7 V_{veh}^2	0.014176	0.001487	9.532381	1.54E-21
a_8	-1.13364	0.282866	-4.00769	6.13E-05

Table 12 Payoff Matrix with Additional Data

		Driver	
		Yield	Do Not Yield
Pedestrian	Cross	$[0.0948v_{ped}^2,$ $0.0802d_{veh} - 0.0003d_{veh}^2]$	[0, -1.295]
	Do Not Cross	$[0.936 - 0.033d_{ped} + 0.00016d_{ped}^2,$ $0.0802d_{veh} - 0.0003d_{veh}^2]$	$[0.936 - 0.033d_{ped} + 0.00016d_{ped}^2,$ $0.014v_{veh}^2 - 1.113]$
Pedestrian (mean case)	Cross	[2.14, 2.136]	[0, -1.113]
	Do Not Cross	[0.09, 2.136]	[0.09, 2.388]

PUBLICATIONS

Fricker, J. D., & Zhang, Y. (2019). Modeling pedestrian and motorist interaction at semi-controlled crosswalks: the effects of a change from one-way to two-way street operation. Transportation research record, 2673(11), 433-446.

Zhang, Y., Qiao, Y., & Fricker, J. D. (2020). Investigating Pedestrian Waiting Time at Semi-Controlled Crossing Locations: Application of Multi-State Models for Recurrent Events Analysis. Accident Analysis & Prevention, 137, 105437.

Zhang, Y., & Fricker, J. D. (2020). Multi-State Semi-Markov Modeling of Recurrent Events: Estimating Driver Waiting Time at Semi-Controlled Crosswalks. Analytic Methods in Accident Research, 100131.

Yabe, T., Zhang, Y., & Ukkusuri, S. V. (2020). Quantifying the economic impact of disasters on businesses using human mobility data: a Bayesian causal inference approach. EPJ Data Science, 9(1), 36.

Zhang, Y., & Fricker, J. D (2021). Investigating temporal variations in pedestrian crossing behavior at semi-controlled crosswalks: A Bayesian multilevel modeling approach. Transportation Research Part F: Traffic Psychology and Behaviour, 76, 92-108.

Zhang, Y., & Fricker, J. D. (2021). Quantifying the impact of COVID-19 on non-motorized transportation: A Bayesian structural time series model. Transport Policy, 103, 11-20.

Zhang, Y., & Fricker, J. D. (2021). Incorporating conflict risks in pedestrian-motorist interactions: A game theoretical approach. Accident Analysis & Prevention, 159, 106254.

Zhang, Y., Fricker, J. (2022). “Forecasting the Motion and Behavior of Heterogeneous Road Users at Crosswalks: A Spatial Temporal Graph-Based LSTM Approach”. Submitted to IEEE International Conference on Robotics and Automation.